Extrinsic Fabry-Perot Interferometer System Using Wavelength Modulated Source

by

Scott A. Meller

Thesis submitted to the Faculty of the
Virginia Polytechnic Institute and State University
in partial fulfillment of the requirements for the degree of
MASTER OF SCIENCE
in
Electrical Engineering

APPROVED:

Anbo Wang, Chairman
Richard O. Claus
Kent A. Murphy

December, 1996
Blacksburg, Virginia

Keywords: Optical fiber sensors, interferometry, multilongitudinal mode laser diode, extrinsic Fabry-Perot interferometer, pseudo-heterodyne modulation

Extrinsic Fabry-Perot Interferometer System Using Wavelength Modulated Source

by
Scott A. Meller

Anbo Wang, Chairman
Electrical Engineering

Abstract

Interferometric optical fiber sensors have proved many orders of magnitude more sensitive than their electrical counterparts, but they suffer from limitations in signal demodulation caused by phase ambiguity and complex fringe counting when the output phase difference exceeds one fringe period. Various signal demodulation methods have been developed to overcome some of the these drawbacks with limited success.

This thesis proposes a new measurement system for the extrinsic Fabry-Perot interferometer (EFPI) sensor. Using a wavelength modulated source and a novel extended-gap EFPI, some of the limitations of interferometric signal demodulation are overcome. By scanning the output wavelength of a multilongitudinal mode laser diode through current modulation, the EFPI sensor signal is scanned through multiple fringes. Gap movement is then unambiguously determined by monitoring the phase of the multiple fringe pattern.

Acknowledgments

I would like to thank all of my committee members for their support and encouragement before and during my time spent at Fiber and Electro-Optics Research Center. Without the help and advice of Dr. Richard Claus and Dr. Kent Murphy, I simply would not exist at Virginia Tech. I would like to thank Dr. Anbo Wang for serving as my advisor and committee chairman, for the many fruitful discussions, and for the valuable guidance and support during the preparation of this thesis.

I have enjoyed working with all the students and researchers at FEORC over the past 2 years. Special thanks to Vivek Arya and Dr. Marten de Vries for serving as my "mentors" and for providing so much useful advice during my research at FEORC.

I also owe a lot of thanks to my parents for their never ending encouragement, love, and support throughout my life. They have provided me with the tools to succeed.

Most importantly, I would like to thank my wife, Angie, for her understanding and love, for enduring the many late nights and grouchy mornings, for helping me achieve my goals in life, and for being a wonderful mother to Drew and Katie.

Table of Contents

List of Illustrations

Chapter 1 - Introduction

Monitoring environmental parameters is an important aspect of many electrical and mechanical systems. Manufacturing systems, aerospace vehicles, civil structure monitoring systems, and medical devices depend on accurate and reliable sensors. Information from sensors are used for active control, calibration, and failure prevention in these systems. Therefore, the system design must include a cost-effective sensor network to monitor environmental parameters.

1.1 Optical Fiber Sensors

Optical fiber sensors are excellent candidates for monitoring environmental parameters because of their numerous advantages over conventional sensors. Some of the advantages include light weight, small size, high sensitivity, immunity to electromagnetic interference, and potential for large-scale multiplexing. The widespread use of optical fiber communication devices by the telecommunication industry has resulted in mass production of associated optical and electrical components that are also used in optical fiber sensor systems. Therefore, economies of scale have produced substantial reductions in optical fiber sensor cost [1].

Many optical fiber sensors have found numerous applications in industry, some of which include fiber optic gyroscopes for automotive navigation systems [2], strain sensors for smart structures [3,4], and a variety of fiber optic sensors for manufacturing and process control [1]. Fiber optic sensors have also been used to monitor a large number of environmental parameters such as position, vibration, temperature, acoustic waves, chemicals, current, and electric field.

1.2 Classification of Optical Fiber Sensors

Optical fiber sensors can be broadly classified as either intrinsic or extrinsic, and more specifically classified by their operating principles. Information in each type sensor can be conveyed by polarization, phase, frequency, wavelength, and intensity modulation, or a combination of the above.

If all sensing mechanisms take place within the fiber itself, the sensor is classified as intrinsic. In this type sensor, the fiber functions as both a transmission medium and sensing element. An external parameter induces a change in the light guiding properties of the fiber which is detected and demodulated to produce measurand information. In extrinsic sensors, the fiber plays no role in the sensing mechanism and only serves to bring the light to and from an external medium where it is modulated. The external medium can range from special optical crystals to air.

1.2.1 Classification by Operating Principle

Optical fiber sensors can be further classified by their operating principle. If the sensor is based on the interference between light waves, it is referred to as interferometric. Interferometric sensors are classified by their geometry; Fabry-Perot, Mach-Zehnder, Michelson, and Sagnac. Other sensors are based on the loss of light from the fiber or coupled to the fiber and are referred to as intensity based sensors. The following sections describe some common fiber optic sensors and their sensing mechanisms.

1.2.1.1 Microbending Sensors

One of the earliest optical fiber sensors developed were microbend sensors [6]. This intrinsic, intensity based sensor utilizes mode coupling in multimode fiber. A fiber mode is a particular light path in the optical waveguide and is uniquely described by its propagation constant, β, and its electric field distribution. Multimode fibers typically contain thousands of possible modes. When a multimode fiber is subjected to periodic small deformations or microbends, energy may transfer from one mode to another. This mechanism is illustrated using ray diagrams in Figure 1.1. Figure 1.1a shows a higher order mode that is traveling close to the critical angle of the fiber which is defined as

$$\theta_c = \sin^{-1}\left(\frac{n_2}{n_1}\right) \tag{1.1}$$

When a bend is induced in the fiber, this ray may exceed the critical angle and is no longer guided (Figure 1.1b).

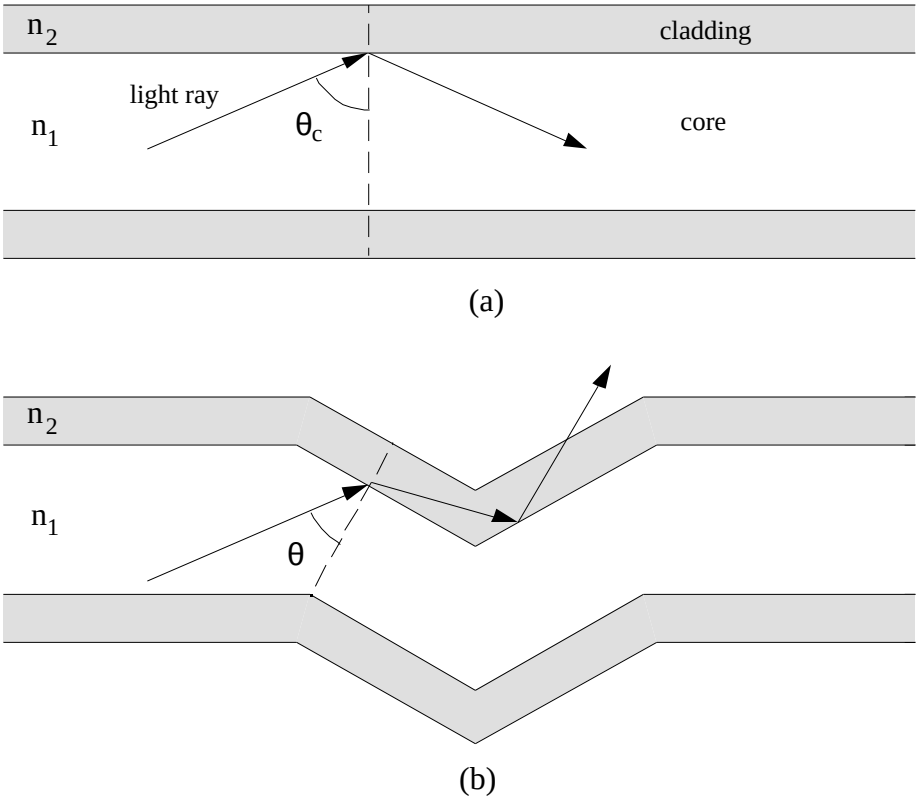

Figure 1.1. Microbending in Multimode Fiber.(a) Ray traveling close to the critical angle, (b) small deformation causing ray to exceed the critical angle

This mode coupling is achieved by placing the fiber between two deformer plates with periodic grooves (Figure 1.2). The period of the grooves (Λ) is determined by the difference between the propagation constants for adjacent modes ($d\beta$) and is given by [6]

$$d\beta = \frac{2\pi}{\Lambda}. \qquad (1.2)$$

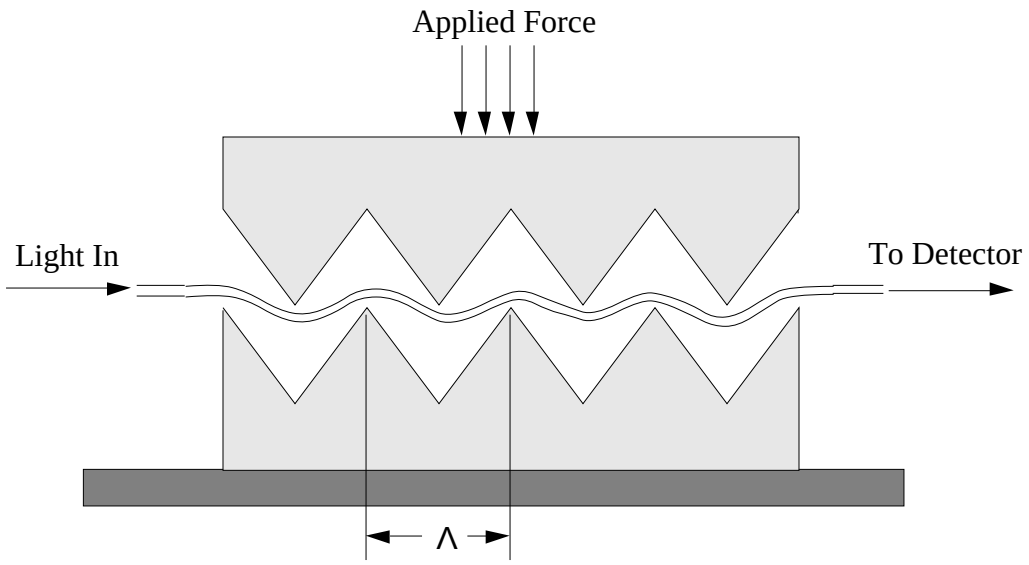

Figure 1.2. Microbend Sensor

For fibers with a graded index of refraction from core to cladding, this mode coupling sharply peaks at groove spacing given by

$$\Lambda = \frac{2\pi a}{(2\Delta)^{1/2}}, \tag{1.3}$$

where a is the fiber radius and Δ is the normalized index difference between the core and the cladding. For fibers with a step index, the loss has a threshold defined by

$$\Lambda \leq \frac{\pi a}{\Delta^{1/2}}. \tag{1.4}$$

Microbend sensors have been successfully employed as displacement, pressure, acceleration, and temperature transducers. Figure 1.3 shows the amplified optical output of a microbend sensor designed for vehicular axle detection [7]. The microbend sensor was installed in a small groove cut into the road surface and backfilled with magnetic induction detector loop sealant. The two intensity drops are from the front and rear wheels of a car traveling at 16 miles per hour. The decrease in intensity is proportional to the axle weight of the front wheel drive car.

Properly designed, a microbend sensor lifetime can exceed 10^{10} cycles [6]. Because it is an intensity based sensor, the optical source and supporting electronics are typically inexpensive compared to other optical fiber sensors. The major drawbacks in this type sensor are its sensitivity to fluctuations in source power and lead-in/lead-out fiber losses. Also, its resolution is moderate compared to more sensitive interferometric sensors.

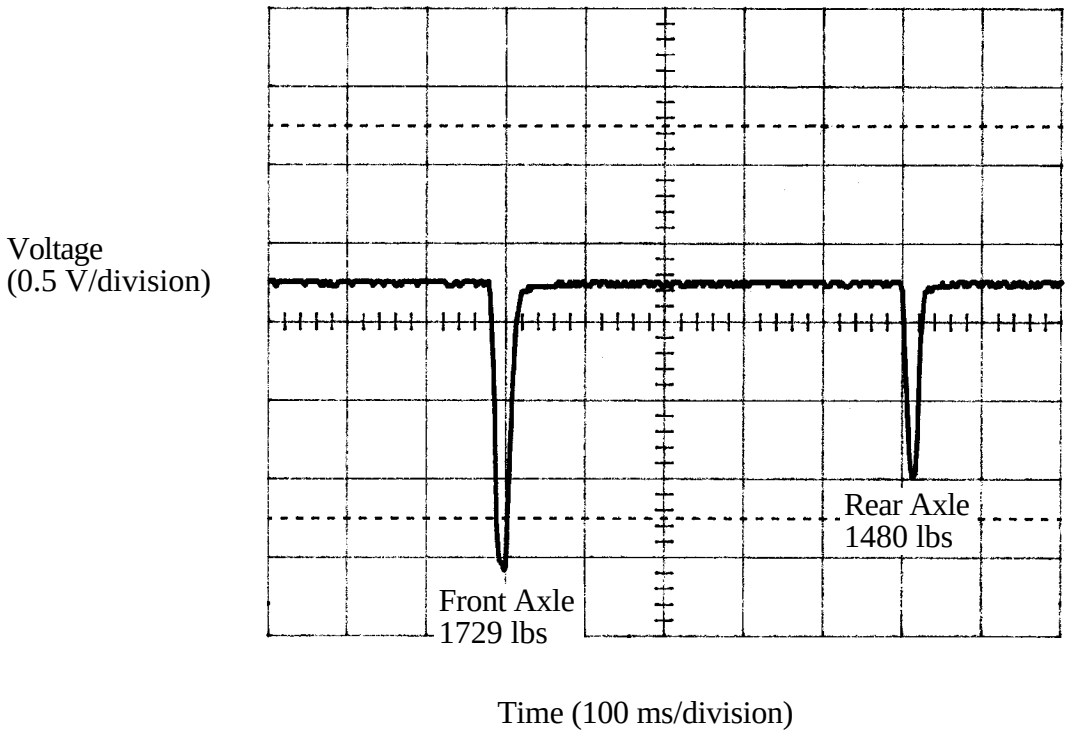

Figure 1.3. Axle Detection Microbending Sensor Output

1.2.1.2 Mach-Zehnder Interferometer

The Mach-Zehnder configuration (Figure 1.4) is an intrinsic sensor based on the interference between a sensing and a reference wave. The two beam interferometer uses a laser diode as the source of coherent light which is coupled into a single mode fiber. The light is then split equally into two fibers by a 3 dB coupler. One leg of the Mach-Zehnder interferometer is the sensing leg while the other is the reference. The reference fiber is kept protected from the desired perturbation to be measured and light passes through this leg

normally. The sensing fiber is used to monitor the perturbation. Two complementary outputs are available for signal processing.

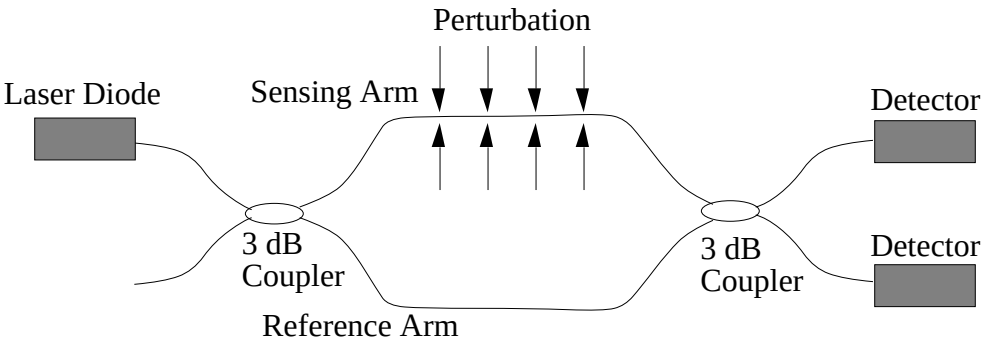

Figure 1.4. Mach-Zehnder Interferometer

The electric fields of the two light waves can be expressed as

$$E_r = E_0 e^{i\omega_0 t}, \tag{1.5}$$

and

$$E_s = E_0 e^{i(\omega_0 t + \Delta\phi)}, \tag{1.6}$$

where E_r is the reference wave, E_s is the sensing wave, and $\Delta\varphi$ is the phase difference induced by the sensing fiber. At the photodetector, the intensity is given by [1]

$$I = \langle E_r^2 \rangle + \langle E_s^2 \rangle + 2\langle E_r E_s \rangle, \tag{1.7}$$

where $\langle\ \rangle$ represents the time integration performed by the photodetector. This Equation reduces to

$$I = I_0\left(1 + \cos\Delta\phi\right), \tag{1.8}$$

where $I_0 \propto E_o^2$ and we have assumed the ideal conditions of equal splitting ratios, no coherence or polarization effects, and no losses.

The information is contained in the phase difference between the two waves. The phase corresponding to a length of fiber L is

$$\phi = k n_e L, \tag{1.9}$$

where k=2π/λ is the propogation constant in air, λ is the laser diode emitting wavelength, and n_e is the fiber's effective refractive index. If the desired measurand is X, then the change in φ may be represented by [5]

$$\Delta\phi = kL\frac{dn_1}{dX}\Delta X + kn_1\frac{dL}{dX}\Delta X \ . \qquad (1.10)$$

If the coefficients $\frac{dn_1}{dX}$ and $\frac{dL}{dX}$ for the sensing fiber are known, ΔX can be found from the output signal, expressed by Equation (1.8).

In this configuration, quantities such as strain, force, pressure, and temperature can be measured directly. Other quantities such as magnetic field, acoustic pressure, electric field, and current can be measured indirectly by attaching the sensing fiber to materials that respond to these parameters.

The output of the sensor, Equation (1.8), is sinusoidal and is shown in Figure 1.5. The signal goes through one period for every 2π shifts in Δφ. This period is referred to as one fringe. The sensor has maximum sensitivity at the quadrature (Q) point.

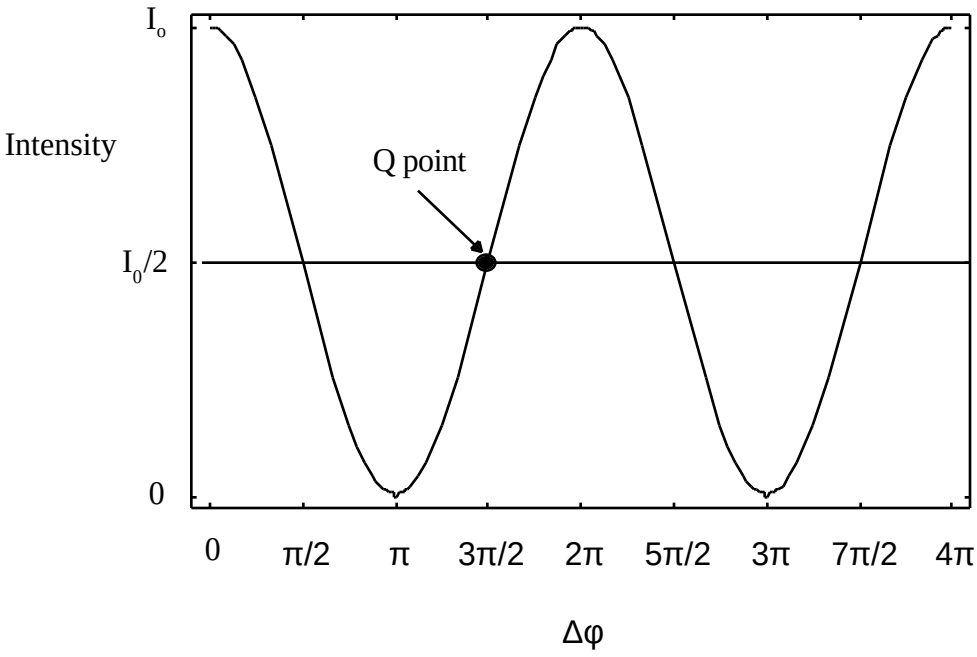

Figure 1.5. Mach-Zehnder Output

Figure 1.5 illustrates a number of difficulties for this sensing scheme:

1. The signal must be maintained around the Q point in order to avoid loss of sensitivity.
2. If the sign of $\Delta\varphi$ changes at a maximum or minimum of the fringe, there is no way of knowing this occurred. Therefore, the sensor also experiences phase ambiguity under these conditions.
3. Because the signal is composed of the phase difference between the sensing and reference arms, no absolute information is available. Upon powering up the system, the initial condition of X, the measurand, cannot be deduced from the signal. The system can only track ΔX.
4. Any wavelength instability in the source will cause a change in the phase because of the k term in Equation (1.10).

These difficulties are characteristics of all interferometric type sensing schemes. Various signal demodulation methods have been developed to overcome some of the these drawbacks of the sensor including active and passive homodyne, differentiate cross multiplication, synthetic heterodyne, and true heterodyne [1].

1.2.1.3 Extrinsic Fabry-Perot Interferometer

The extrinsic Fabry-Perot interferometer (EFPI) is an optical fiber sensor based on the combination of two light waves, similar to the Mach-Zehnder configuration described previously. As seen in Figure 1.6, the EFPI consists of an input/output fiber, and a reflector fiber aligned by a hollow core silica tube [9].

The EFPI can be approximated as a two beam interferometer. The laser diode light arrives at the sensor head and a portion is reflected off the fiber/air interface (R1). The remaining light propagates through the air gap (L) and a second reflection occurs at the air/fiber interface (R2). R1 is the reference reflection while R2 is the sensing reflection. These two light waves interfere constructively or destructively based on the path length traversed by the sensing reflection, and travel back through the coupler to the detector. The second output of the coupler is shattered to prevent reflections from interfering with the EFPI signal. Small movements in the hollow core cause a change in the gap distance, which changes the phase

difference between the sensing and reflecting waves. If the hollow core tube is attached to a material, and the gauge length of the sensor is known, strain in the material can be accurately measured.

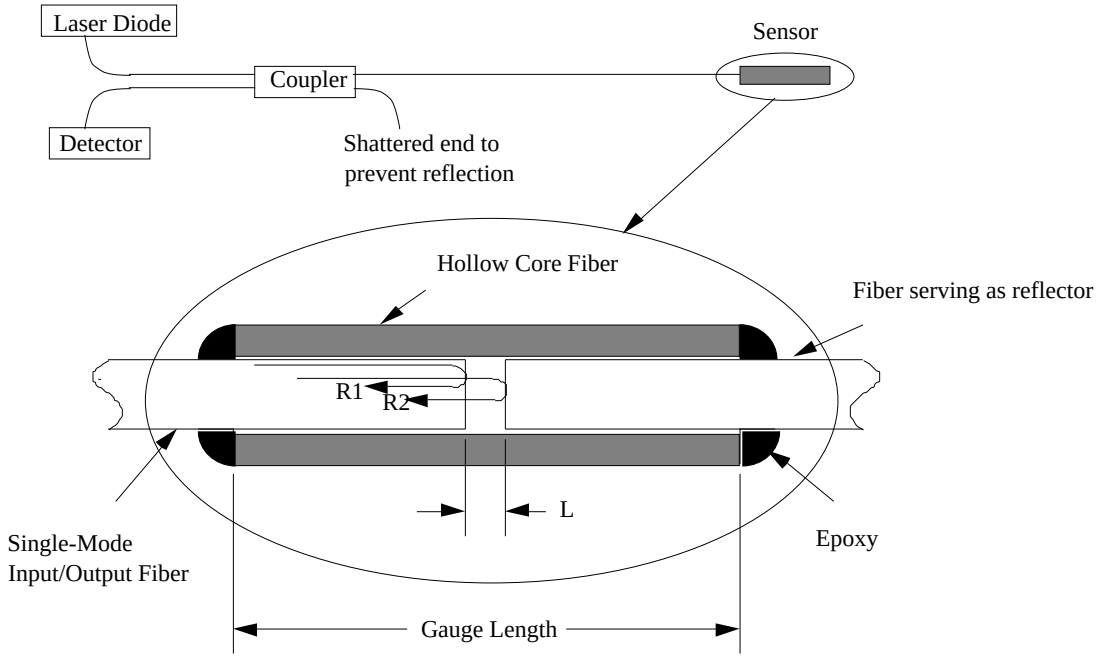

Figure 1.6. The Extrinsic Fabry-Perot Interferometer

If A_1 and A_2 are the amplitudes of the two waves and $\Delta\varphi$ is the phase difference between them, the intensity at the detector is given by

$$I_r = |A_1 + A_2|^2 = A_1^2 + A_2^2 + 2A_1A_2\cos\Delta\phi \qquad (1.11)$$

A typical output of the EFPI sensor is shown in Figure 1.7. A phase change of 360 degrees in the sensing reflection corresponds to one fringe period. At a wavelength of 1.3 μm, the change in gap for one fringe period is 0.65 μm. The drop in detector intensity is due to the decrease in coupled power from the sensing reflection as it travels farther away from the single-mode input/output fiber.

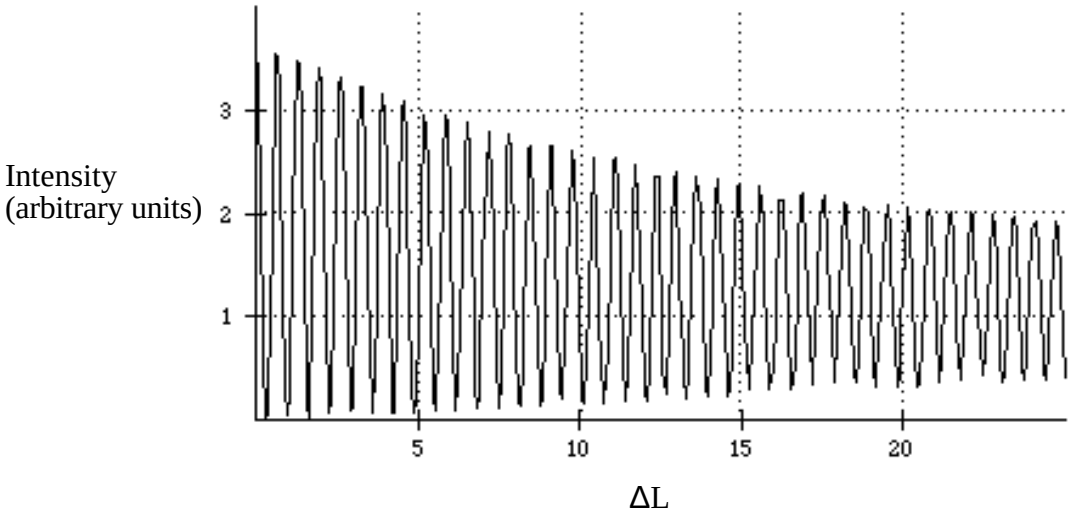

Figure 1.7. EFPI output for 25 μm change in gap

The EFPI, because it is an interferometric sensor, suffers from the same limitations as mentioned for the Mach-Zehnder configuration. Because it is an extrinsic sensor, the methods used to overcome these limitations are different. The current methods employed are quadrature phase shifted operation, dual wavelength method, and white light interferometry.

1.3 Thesis Objective and Overview

The goal of this thesis is to propose, design, and implement a new measurement system for the EFPI sensor. Using a wavelength modulated source and a novel extended-gap extrinsic Fabry-Perot interferometer (EG-EFPI), some of the limitations of interferometric signal demodulation are overcome.

Chapter 2 covers the non-ideal considerations of the EFPI and the current demodulation schemes. Chapter 3 presents the theoretical background of the wavelength modulation technique. The extended-gap configuration is also presented with the signal demodulation approach. Chapter 4 describes the experimental set-up, some of the limitations encountered, and covers the results and characteristics of the wavelength modulated EG-EFPI system.

Chapter 2 - The EFPI and Improved Signal Measurement Schemes

The EFPI sensor can be configured to measure a number of different parameters including strain, temperature, surface acoustic waves, and pressure. In each configuration, the measurand imparts a change in the gap spacing between the reference and reflection fibers.

The output signal of the EFPI is in the form of fringes and contains directional ambiguity, non-linearities, and no absolute gap distance information. If the signal is not maintained around the Q point, the sensitivity and accuracy of the sensor degrades. The decrease in coupled power from the sensing reflection as it travels farther away from the single-mode input/output fiber, further degrades sensitivity and accuracy. If the direction of gap movement changes at the maximum or minimum of a fringe, there is no way of knowing this occurred. Because the signal consists of the change in phase between the sensing and reference waves, it is differential and contains no absolute gap information. Upon system power-up, there is no way of knowing the initial conditions of the gap from the sensor signal.

As a result of the signal demodulation difficulties above, several improved systems have been developed that provide absolute gap distance information and/or unambiguous information about the direction of gap movement. Each method has trade-offs in resolution, system complexity, dynamic range, and dynamic response. The improved sensing schemes covered are quadrature phase-shifted EFPI, two wavelength method, and white-light interferometry. Particular attention is paid to their accuracy, resolution, dynamic response, and system complexity. The non-ideal considerations of the EFPI signal are covered first followed by the improved signal demodulation schemes.

2.1 Non-ideal considerations of the EFPI

Ideally, the EFPI is a two beam interferometer whose output is given by Equation (1.11). In reality, a number of non-ideal factors must be taken into account when demodulating the EFPI signal. The two primary considerations are the two beam interferometer approximation and decreased coupled power from the sensing reflection.

2.1.1 Two beam approximation

The normalized received intensity of a Fabry-Perot cavity in reflection is [8]

$$I_r = \frac{1-\cos\Delta\phi}{1+R^2-2R\cos\Delta\phi}, \tag{2.1}$$

where R is the power reflectivity of the interfaces between glass and air. In the two beam approximation, the denominator is taken to be one since R is small (~0.035) for a low finesse cavity, and the output becomes

$$I_r \approx 1-\cos\Delta\phi. \tag{2.2}$$

This approximation introduces error in the determination of phase which is used to determine the change in gap by

$$\Delta\phi = \frac{4\pi\Delta L}{\lambda} \tag{2.3}$$

Equations (2.1) and (2.2) are plotted for different values of $\Delta\varphi$ in Figure 2.1. The maximum error induced in phase determination occurs when $\Delta\varphi = 2(m+1/2)\pi$, m being an integer. The maximum error is 6.5% for R = 0.035 [8]. The minimum error occurs at intervals of $\pi/2$ which is also the Q point.

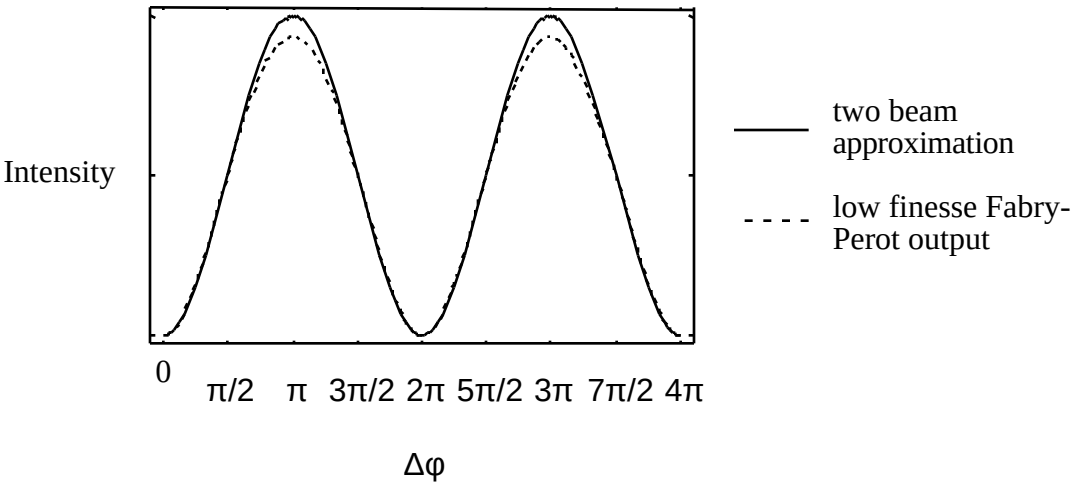

Figure 2.1. Low finesse Fabry-Perot output and two beam approximation

2.1.2 Decrease in sensing reflection coupled optical power

The EFPI also deviates from the ideal two beam approximation because of the decrease in coupled power from the sensing reflection. The decrease in coupled power can be approximated in Equation (1.11) by redefining A_2 using a simplified loss relation as [9]

$$A_2 = A_1\left(\frac{ta}{a + 2L\tan[\sin^{-1}(NA)]}\right), \tag{2.4}$$

where a is the fiber core radius, L is the gap, t is the transmission coefficient of the air glass interface, and NA is the numerical aperture given by

$$NA = \left(n_1^{\,2} - n_2^{\,2}\right)^{1/2}, \tag{2.5}$$

and n_1, n_2 are the core and cladding refractive indexes respectively. Substituting Equation (2.4) into Equation (1.11) yields

$$I_r = A_1^{\,2}\left(1 + \left(\frac{ta}{a + 2L\tan[\sin^{-1}(NA)]}\right)^2 + \frac{2ta}{a + 2L\tan[\sin^{-1}(NA)]}\cos(\Delta\phi)\right). \tag{2.6}$$

Equation (2.6) is plotted in Figure 2.2. From this plot we can see that as the gap increases, the sensitivity and signal to noise ratio also decrease. A measure of the available signal is the fringe visibility which is defined as

$$V = \frac{I_{\max} - I_{\min}}{I_{\max} + I_{\min}}. \tag{2.7}$$

As the gap increases, the fringe visibility decreases.

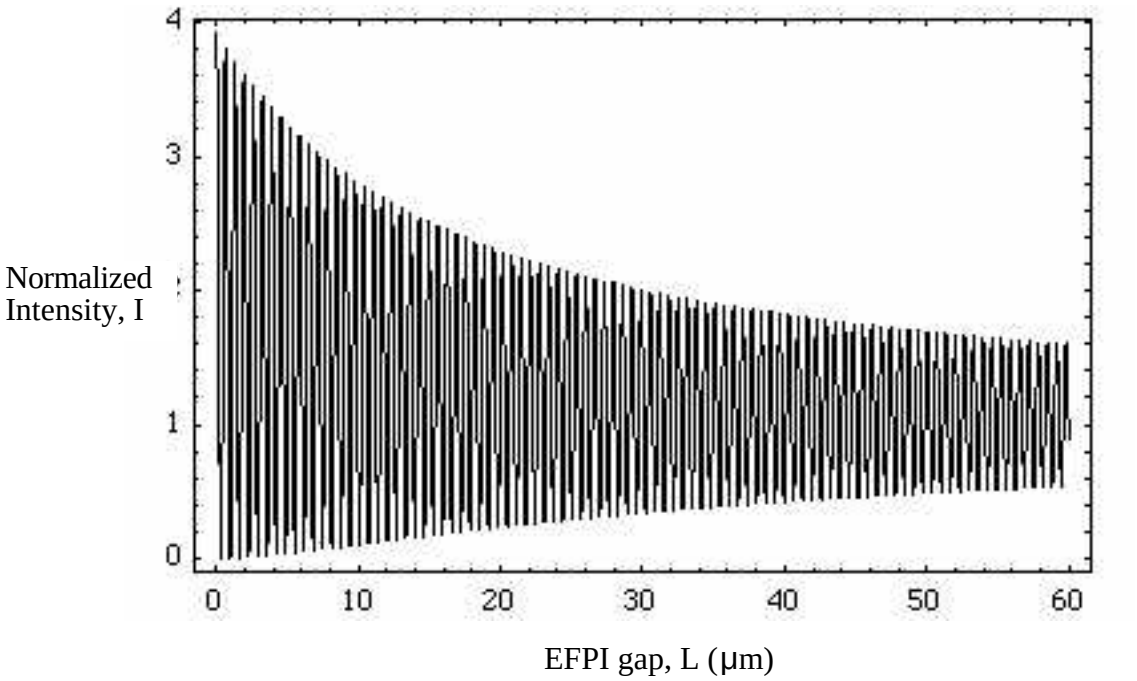

Figure 2.2. EFPI output with sensing reflection coupling loss

In summary, the EFPI signal must be maintained around the Q point in order to obtain accurate information about the gap. If the particular sensing application demands a large dynamic range of operation, then the EFPI output will scan through multiple fringes and complex fringe counting methods must be employed. Sensors tested with the fringe counting method have shown 0.01μstrain resolution with a 19.03 mm gauge length, corresponding to an absolute measurement resolution of 0.19 nm and a strain sensitivity of 91.3 x 10^{-3} radians/με - cm [10].

2.2 Improved Signal Demodulation Schemes

The following methods have been implemented to improve signal demodulation of the EFPI.

2.2.1 Quadrature Phase Shifted EFPI

The quadrature phase shifted EFPI [9] allows unambiguous information about the direction of gap movement, but complex fringe counting must still be employed. In this method, a

special sensor head is designed to give two signals π/2 out of phase or in quadrature with each other. The arrangement of this sensor is shown in Figure 2.3.

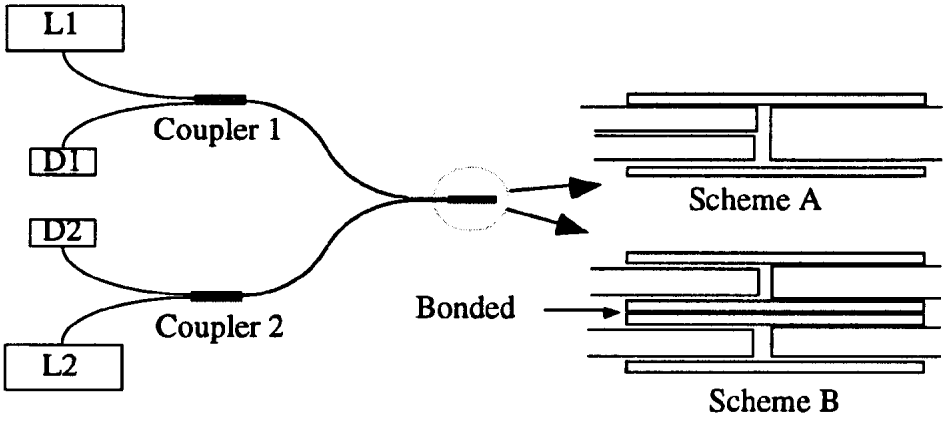

Figure 2.3. Arrangement for quadrature phase shifted EFPI

The system consists of two input/output fibers with two separate sources. The two input/output fibers are bonded close together via scheme A or B such that a difference in each sensors gap length causes their signals to be in quadrature. In this way, one sensor is always at the quadrature point when the other is at a point of minimum sensitivity (Figure 2.4). By monitoring the phase lead-lag of the two signals, unambiguous directional information can be obtained.

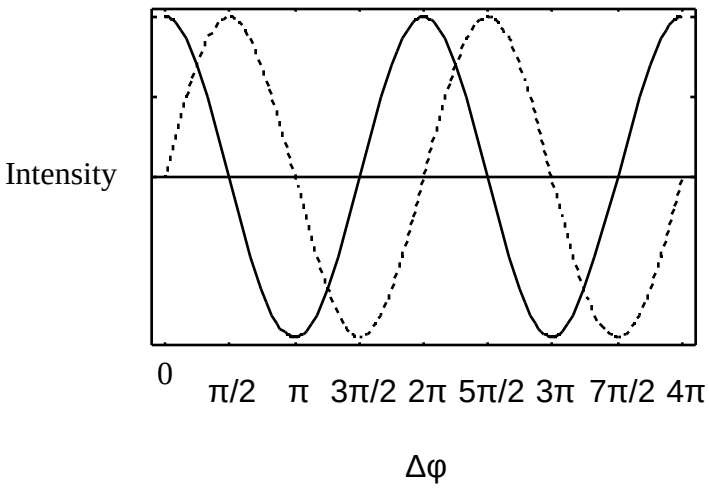

Figure 2.4. Two signals in quadrature

To obtain ΔL, complex fringe counting methods still must be employed. In addition, sensor fabrication is difficult because the difference in gap separation is small. For the signals to be in quadrature [11]

$$L_1 - L_2 = (2n+1)\frac{\lambda}{8}\ , \tag{2.8}$$

which is difficult to achieve and maintain. The signals could come out of quadrature under cyclic strain conditions.

2.2.2 Dual Wavelength Method

Another method for unambiguously detecting gap movement direction is the dual wavelength approach. This method, unlike the quadrature phase shifted EFPI, utilizes only one sensor head, but compromises the dynamic range of the measurement system.

If the EFPI is illuminated with two sources of wavelengths λ_1 and λ_2, the output phase signal generated by each wavelength is [12]

$$\Delta\phi_1 = \frac{4\pi L}{\lambda_1}, \tag{2.9}$$

and,

$$\Delta\phi_2 = \frac{4\pi L}{\lambda_2}. \tag{2.10}$$

The relative phase difference between the two signals is then

$$\Delta\Phi = 4\pi L\,\frac{\Delta\lambda}{\lambda_1\lambda_2}, \tag{2.11}$$

where $\Delta\lambda$ is λ_1 - λ_2. The dynamic range is limited to $0<\Delta\Phi<\pi$ radians. In terms of maximum gap displacement,

$$\Delta L_{max} = \frac{\lambda_1\lambda_2}{8\Delta\lambda}. \tag{2.12}$$

A typical dynamic range for this system is 40 μm.

For a given dynamic range, monitoring the phase lead-lag of the two signals yields unambiguous directional information. Figure 2.5 shows the phase lead-lag relationship of an EFPI interrogated with two source wavelengths. At time t_1, the direction of gap

movement changes. Fringe counting methods must still be employed to get accurate ΔL information.

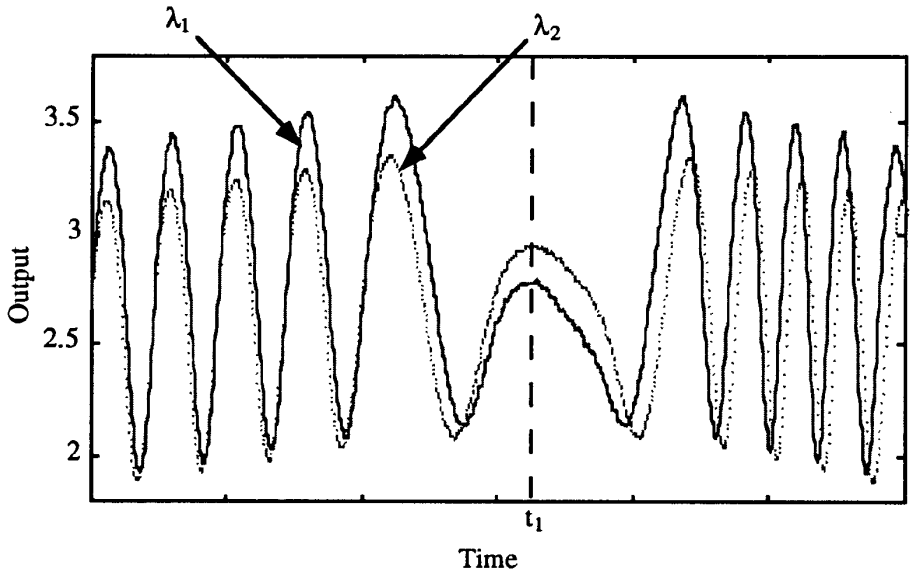

Figure 2.5. Output of dual wavelength system [12]

2.2.3 White-light Interferometry Technique

The white-light interferometry technique allows absolute gap length detection. The EFPI is illuminated with a broadband source, such as a light emitting diode, and the output is fed into an optical spectrum analyzer (Figure 2.6). Wavelengths for which the phase difference between the sensing and reference reflections are $2n\pi$ will interfere constructively and be maximum. The gap length is then determined from [11]

$$L = \frac{\lambda_1 \lambda_2}{2(\lambda_1 - \lambda_2)}. \tag{2.13}$$

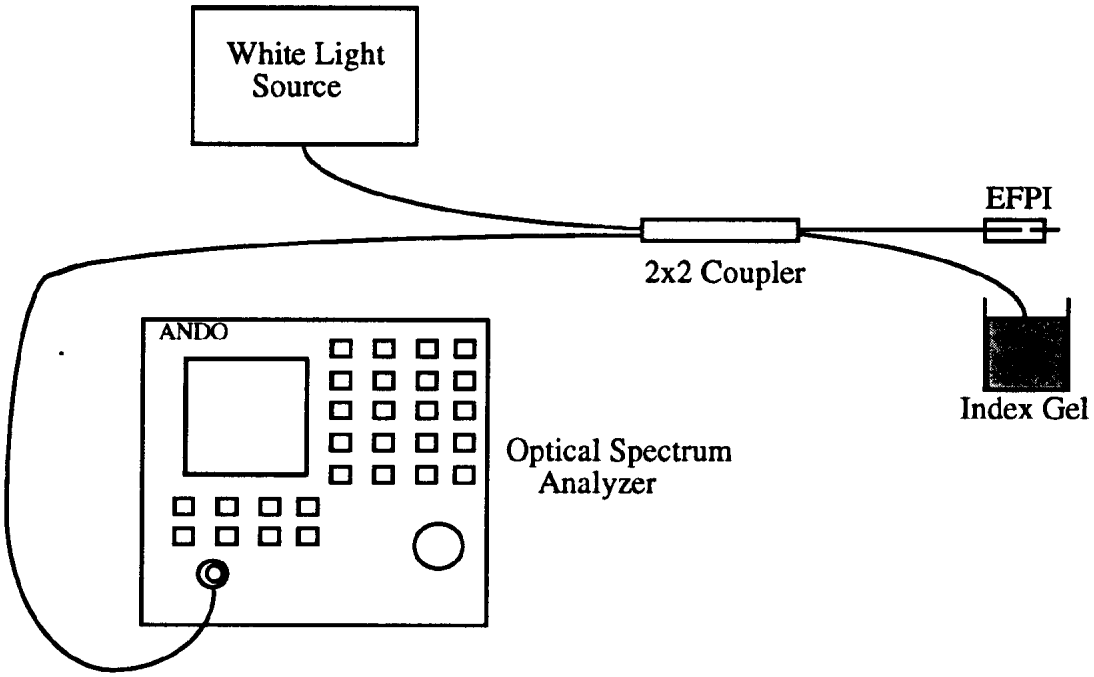

Figure 2.6. Setup for white light interferometry [11]

This method has many advantages including illumination of fringe counting and absolute gap length detection. Using an optical spectrum analyzer for signal demodulation causes the system to have a slow frequency response of 5 Hz and limits measurements to quasi-static gap length changes. In addition, to obtain accurate absolute gap information, the system must be operated in transmissive mode with a high finesse EFPI cavity. This complicates fabrication and the advantages of a single ended sensor are lost. In the system described, the minimum detectable gap length change was 1μm and dynamic range from 0 to 500 μm [11].

Chapter 3 - Wavelength Modulated EFPI Sensor Addressing

The goal of this thesis is the implementation and testing of a new measurement system for the EFPI sensor that will overcome some of the limitations of the current demodulation schemes. Ideally, the new sensing scheme should:

1) Eliminate the need for complex fringe counting.
2) Eliminate the effect of intensity fluctuations on measurement.
3) Have sufficient dynamic response.
4) Have sufficient resolution.
5) Maintain a simple cost effective design.
6) Eliminate directional ambiguity
7) Provide absolute gap length information

To achieve this we employ a method utilizing wavelength modulation of the source. Laser diodes are excellent sources for use in this sensor demodulation scheme because of their cost effectiveness, efficiency, small size, and wavelength modulation capabilities. It is well known that the center wavelength of a laser diode varies with injection current and junction temperature. By applying a current modulation to the laser diode DC bias current, the output wavelength can by modulated. Gap information can be obtained by continuously sweeping the wavelength through multiple fringe periods[20,21,22,23]. This method is referred to as the frequency modulated continuous wave (FMCW) technique[1]. The term "frequency" may be misleading as the source wavelength is being modulated, but the two are interrelated as

$$\Delta\lambda = \frac{\Delta\nu\lambda_0^{\,2}}{c}, \tag{3.1}$$

with c as the speed of light and λ_0 as the center wavelength. To avoid confusion, hereafter the method will be referred to as wavelength modulation or wavelength sweeping.

3.1 Wavelength Modulation Scheme

The wavelength modulation approach is explained by describing the characteristics of an ideal source that would satisfy all the goals of the work, and then discussing the realistically achievable system.

3.1.1 Ideal Wavelength Modulated Scheme

The ideal source would be capable of shifting the output wavelength by a large amount without any intensity fluctuations. The shift in wavelength must be linear with respect to time and capable of occurring at a fast rate to maximize the frequency response of the system.

To determine wavelength modulation requirements, we investigate the number of fringe periods generated for a particular gap and change in source output wavelength. We derive the wavelength modulation that will scan the output through one fringe period. If λ_1 is some wavelength in which the output is at the minumum of a fringe then

$$m\lambda_1 = OPD, \tag{3.2}$$

where m is an integer and OPD is the optical path difference between the sensing and reflecting waves of the EFPI caused by the distance traveled by the sensing wave. The next fringe peak occurs at some wavelength λ_2 such that

$$(m+1)\lambda_2 = OPD. \tag{3.3}$$

Assuming the OPD remains the same during the wavelength scan time, we can combine (3.2) and (3.3) and solve for m yielding

$$m = \frac{\lambda_2}{\Delta\lambda}, \tag{3.4}$$

where $\Delta\lambda = \lambda_1 - \lambda_2$. Substituting (3.4) into (3.2) results in

$$\Delta\lambda = \frac{\lambda_0^{\,2}}{OPD}, \tag{3.5}$$

where the difference in the two wavelengths is assumed small, thus $\lambda_1\lambda_2 \approx \lambda_0^{\,2}$, and λ_0 is the central wavelength.

If the total change in wavelength or wavelength deviation is $\Delta\lambda_{mod}$, then the number of fringe periods N is

$$N = \frac{\Delta\lambda_{mod}}{\Delta\lambda}, \tag{3.6}$$

and combining Equations (3.5) and (3.6) we have

$$OPD = \frac{N\lambda_0^{\,2}}{\Delta\lambda_{mod}}. \tag{3.7}$$

Thus for an ideal absolute system, λ_o and $\Delta\lambda_{mod}$ are known, and the gap length is determined by monitoring the number of fringe periods appearing for each sweep in wavelength.

3.1.2 Realistic Wavelength Modulation Scheme

To determine the feasibility of this absolute system, we must calculate the minimum wavelength sweep required for at least one fringe period in a typical EFPI. The EFPI is usually made with a gap length L ≈ 50 - 100 μm to maximize fringe visibility and still have adequate dynamic range. Using L = 100 μm and λ_0=1300 nm, $\Delta\lambda_{mod}$ must be at least 8.5 nm to generate one fringe. There are two problems with this approach. A laser diode source with a wavelength sweep of 8.5 nm is not available, and only generating one fringe period does not allow absolute gap measurements since the change in fringe period is small over the operating range of the EFPI.

Although we cannot realistically achieve an absolute system with this approach, it is possible to achieve the first six goals of this work. If one full fringe period can be achieved, the phase of the fringe can be tracked to determine the change in the gap.

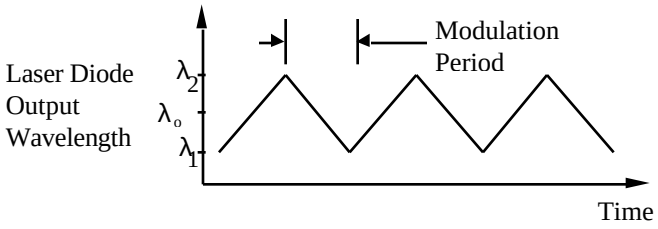

Figure 3.1. Output wavelength versus time for wavelength modulated source.

Figure 3.1 represents the modulation parameters of the laser diode. The central output wavelength is λ_o , and $\Delta\lambda_{mod}=\lambda_2-\lambda_1$. The inverse of the modulation period is defined as

f_{mod}. During each modulation period, there are N fringes appearing at the output. The output of this approach can be represented by

$$I = A\cos\left(2\pi N f_{\text{mod}} t + \Delta\phi\right). \tag{3.8}$$

The variable A is the amplitude of the signal, and $\Delta\varphi$ is the phase change caused a change in L which can be represented by

$$\Delta\phi = \frac{4\pi}{\lambda_0}\Delta L. \tag{3.9}$$

The sign of $\Delta\varphi$ is determined by the direction of ΔL. Using a phase tracking scheme [17], the change in gap length can be accurately determined without directional ambiguity.

It is immediately apparent that goals 1), 2), and 6) are satisfied using a wavelength modulated EFPI addressing scheme. Since the phase contains the gap information, fringe counting is not used. Intensity modulations in the signal input/output fiber will not effect the system provided their frequency is much less than f_{mod}. Likewise, the amplitude of the signal does not effect the accuracy of the system provided the signal to noise ratio is sufficient for the phase tracking method. Therefore, coherence and coupling effects are minimized. Directional ambiguity has been eliminated because the sign of the phase changes with the direction of gap movement.

In order to realize this scheme, we must determine the wavelength sweeping capabilities available in a cost effective source and redesign the EFPI geometry to extend the gap and hence the OPD to obtain at least one full fringe period.

The next sections will discuss wavelength modulation with a laser diode source and present the characteristics of the laser diode used for these experiments. We then discuss the method used to extend the gap of the EFPI. Lastly, important interference considerations are presented.

3.2 Laser Diode Wavelength Modulation Non-Ideal Characteristics

The output wavelength of a laser diode is shifted by two primary effects, current induced changes in the junction temperature, and charge carrier induced refractive index changes. The thermally induced changes are a result of thermal expansion of the Fabry-Perot laser

cavity and thermally induced changes in the refractive index, which combine to increase the output wavelength with increasing injection current. Figure 3.2 shows the increase in laser diode output wavelength for three forward currents of 50, 60, and 70 mA. Since the forward current is modulated, the cavity gain also changes and results in an output intensity modulation in addition to the wavelength modulation.

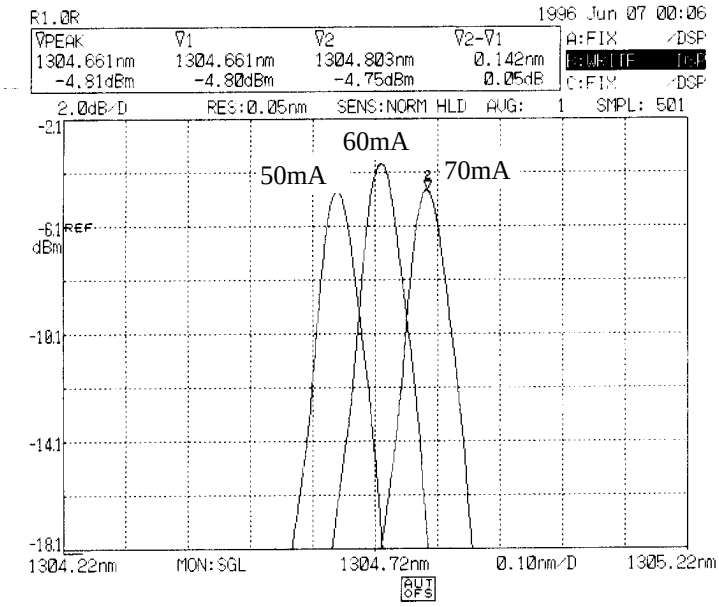

Figure 3.2. Output wavelength of one laser diode mode for three forward currents of 50,60, and 70 mA.

Thermal effects are dominant at modulation frequencies (f_{mod}) below 100 KHz, and are strongly dependent on the laser diode heat sinking and the device structure. The change in wavelength versus forward current is generally non-linear. The frequency deviation is approximately 3 GHz per mA of forward current at 830nm, which is 6.89 pm/mA [13].

Often a peltier element is used in conjunction with a heat sink for the temperature control of the laser diode. As a result, there are 3 different time constants associated with the transfer of heat from the laser diode junction. The chip, submount, and heat sink have time constants range from 0.3 μs to 2.3 ms [14][15], and contribute to the non-linear change in wavelength with injection current.

The laser diode wavelength sweep can be improved by extending the frequency response and linearizing the output. An input equalization network derived from accurate modeling of the thermal constants can extend the frequency response of the thermal effect to 300 KHz [14]. In addition, the wavelength sweep can be linearized through a feedback network that controls the modulation current waveform [16].

As f_{mod} increases above 1 MHz, the thermal effects are negligible and the charge carrier induced refractive index change dominates. The output frequency deviation is much less than the thermal effect. For an 830 nm laser diode, the frequency deviation is a few tenths of gigahertz per mA of forward current [13].

For this sensing scheme, we modulate the laser diode below 100 KHz to maximize the change in output wavelength.

3.3 ML7881A Source Characteristics

The source chosen for these experiments is a Mitsubishi ML7781A multilongitudinal mode laser diode with a central wavelength of 1303 nm. Compared to other available laser diodes, this device had the largest wavelength deviation with the minimum output intensity fluctuation. Figure 3.3 shows the wavelength deviation for the ML7781A laser diode for a slowly increased forward current and shows its non-linear sweep.

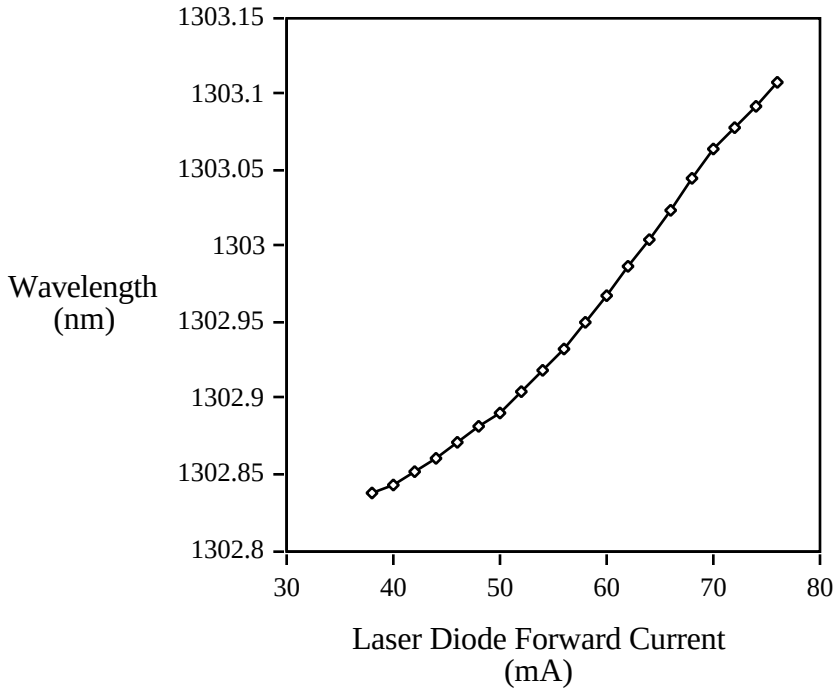

Figure 3.3. ML7781A central wavelength vs. forward current

The maximum available wavelength deviation is 0.25 nm for a forward current modulation of 37 mA (6.7 pm/mA).

The ML7781A is a multilongitudinal mode device and hence has multiple peaks in the output spectrum shown in Figure 3.4.

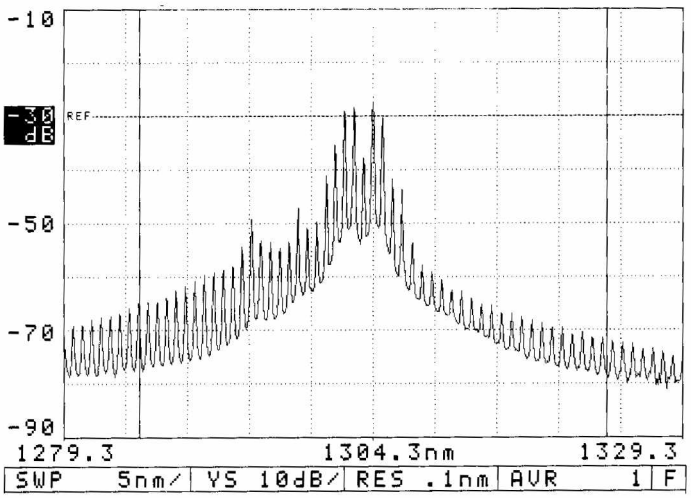

Figure 3.4**.** ML7781A at 60 mA T=25c

3.4 Extended-gap EFPI

Although it is possible to obtain a larger wavelength deviation using an external-cavity laser diode or a dye laser, these devices at present are not cost effective and their maximum modulation frequency is limited. Therefore, we must increase the OPD of the EFPI to create one fringe.

Assuming we can achieve a reasonably linear wavelength deviation of 0.125 nm with the ML7781A source, the gap required for one full fringe is 1.35 cm. At this gap, coupling loss and coherence effects cause the fringe contrast to decrease substantially, and hence the signal to noise ratio to be poor. Figure 3.5 shows the decrease in the peak-to-peak fringe output of the EFPI as the gap is scanned from 0 to 500μm.

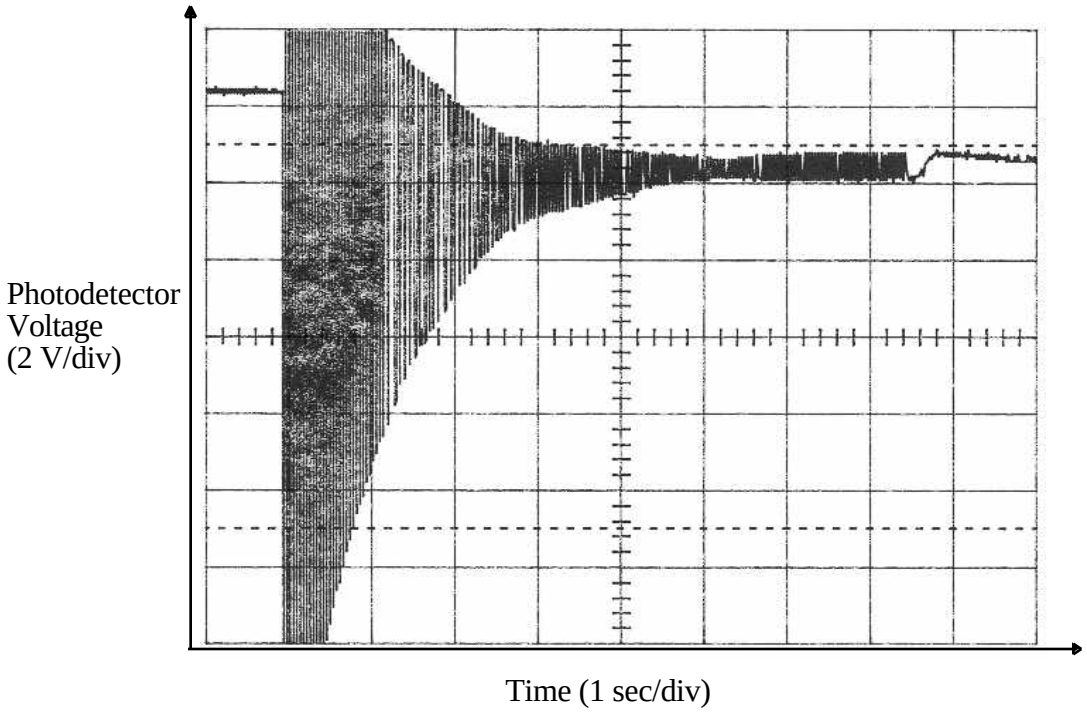

Figure 3.5 Fringe output of EFPI as the gap is increased from 0 to 500μm.

To increase the signal to noise ratio, a novel extended-gap EFPI sensor geometry is employed (Figure 3.6). The input light from the single mode fiber is reflected at the first air-to-glass interface to form the reference reflection, R1. The remaining light travels through the small air gap and is reflected off the reflector fiber with a surface which is polished at an angle. R2 is not coupled back into the input/output fiber because it now exceeds the acceptance angle of that fiber, and it therefore does not interfere with R1. The remaining light is coupled into the single mode reflector fiber. R3, at the reflector fiber glass-to-air interface, forms the sensing reflection for this geometry, and R4 is reflected out of the fiber like R2.

The requirement for the polished angle at the reflector fiber is such that it exceeds the acceptance angle of the single mode input/output fiber. This is typically 6°-8°. A polished angle of 10° is sufficient to render the effects of R2 and R4 negligible [18,24].

By keeping the air gap small, the coupled power to the reflector fiber is large, and the signal to noise ratio improved. Since the index of refraction for the reflector fiber is 1.46, an OPD of 1.35cm corresponds to a reflector fiber length of 0.925 cm.

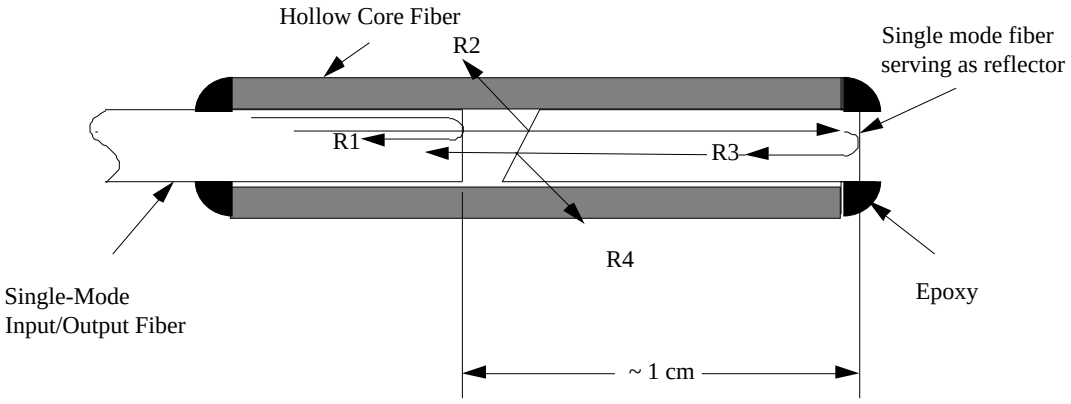

Figure 3.6 Extended-gap EFPI geometry.

Although the extended-gap EFPI allows a wavelength modulated addressing scheme to be employed, it does introduce unwanted cross-sensitivity effects. Since the refractive index of fiber changes with temperature, the OPD in the reflector fiber will also change and cause errors in the output. Equation (3.8), the output of the EFPI with a wavelength modulated source, can be modified to include the temperature dependence as

$$I = A\cos\left(2\pi N f_{\text{mod}} t + \Delta\phi + \Delta\phi_T\right), \tag{3.10}$$

where

$$\Delta\phi_T = \frac{4\pi}{\lambda_0} S\Delta T \frac{dn}{dT}, \tag{3.11}$$

and S is the length of the reflector fiber, ΔT is the change in temperature. Using dn/dT = 10^{-5}/°C, ΔT=10° C, and S = 1cm, $\Delta\phi_T$ = 9.7 radians. Therefore, this geometry is limited to constant temperature applications, or must be temperature compensated.

3.5 Interference zones caused by multilongitudinal mode laser diode

In order to understand the effect a multilongitudinal mode laser diode has on the operation of the EFPI, we must first look more closely at source temporal coherence and autocorrelation.

Instead of viewing the operation of the EFPI as a function of phase, we can redefine everything in terms of time. If we view the source as perfectly monochromatic we can represent its electric field as

$$f(t) = A\sin(2\pi f_o t). \tag{3.12}$$

The output of the EFPI is then the autocorrelation function R(τ) defined as [13]

$$R(\tau) = < f(t) f(t+\tau) >, \tag{3.13}$$

where the roundtrip delay time of the sensing reflection R2 defines τ, and the <> is the time average operation performed by the detector. Substituting Equation (3.12) into (3.13) and evaluating yields

$$R(\tau) = \frac{A^2}{2}\cos(2\pi f_o \tau), \tag{3.14}$$

where we have assumed equal intensities in R1 and R2. This fringe output would have constant amplitude and period of $1/f_o$. In reality, the source has a finite linewidth with a full width half maximum (FWHM) defined by df in Figure 3.7 and is assumed to be Lorentzian distributed. The output can be modified to include the effect of finite linewidth as [17]

$$R(\tau) = \frac{A^2}{2}\cos(2\pi f_o \tau) e^{\left(-\frac{\tau}{2\tau_c}\right)}, \tag{3.15}$$

where τ_c is the source coherence time defined as

$$2\tau_c = \frac{1}{df}. \tag{3.16}$$

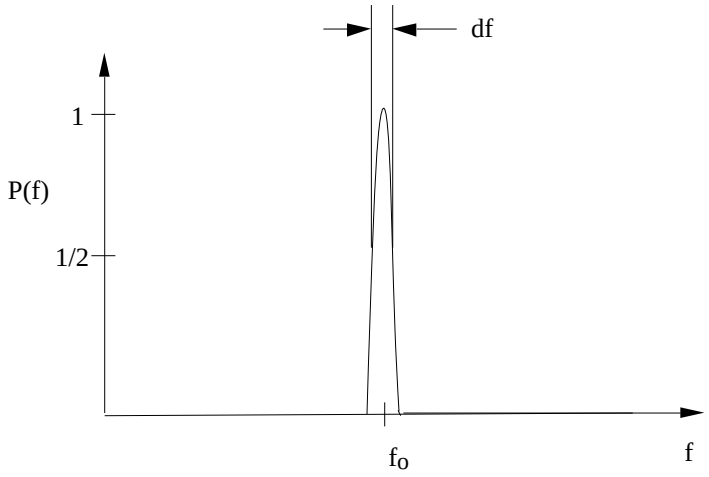

Figure 3.7 Typical spectrum of single longitudinal mode laser.

The output of the EFPI with this source is an interference pattern whose fringe periods are spaced $1/f_0$ apart in time and whose envelope decreases exponentially according to the source coherence time (Figure 3.8).

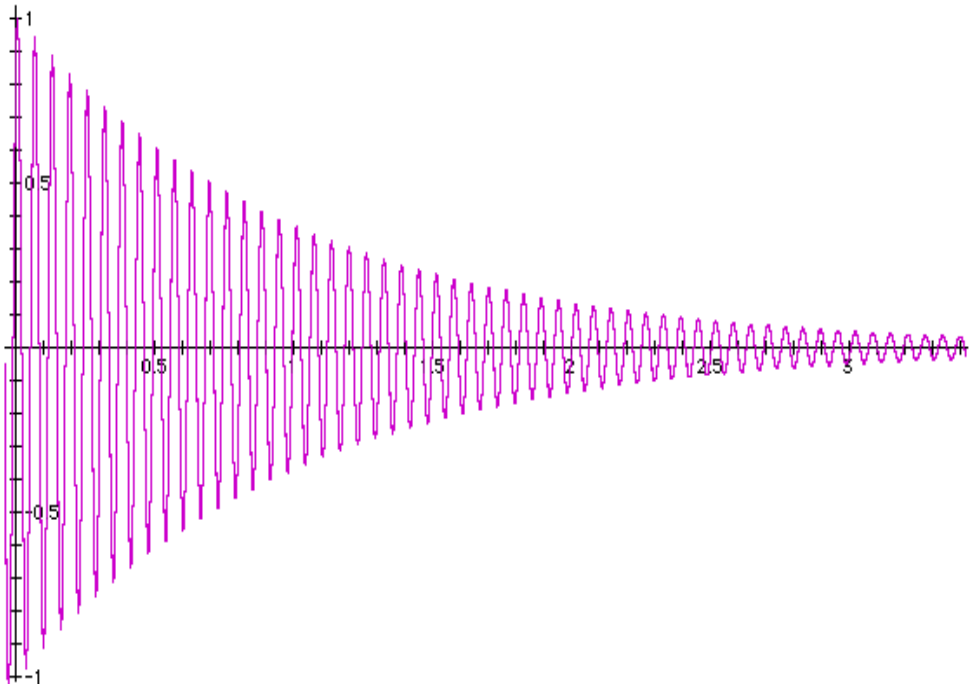

Figure 3.8 Typical fringe output of source as in Figure 3.7.

Looking again at Equation (3.13), the Wiener-Khinchin theorem states that the Fourier transform of the autocorrelation function for f(t) is the power spectral density of f(t). In other words, Figure 3.7 and Figure 3.8 are Fourier transform pairs. In fact, this is a powerful tool for determining the spectrum of a source and is referred to as Fourier transform spectroscopy [18]. With this information, we can now determine the effect a multilongitudinal mode laser will have on the EFPI output.

A typical spectrum of a multilongitudinal mode laser is as shown in Figure 3.9, where df is the mode FWHM, Δf is the power spectrum FWHM, and δf is the mode spacing. Using the inverse relation between Fourier transform pairs, an interference pattern can be derived and is shown in Figure 3.10 [19]. The output pattern consists of a series of equally spaced interference zones with widths $1/\Delta f$, spaced at $1/\delta f$, and with an overall decreasing envelope out to the mode coherence time (1/df). Within each interference zone are fringe oscillations with a period of $1/f_0$. Assuming Lorenztian profile modes, the envelope of the interference zones is $e^{-(t\ df)}$. The profile of Δf is due mainly to spontaneous emission and is Gaussian distributed so the envelope of each interference zone is described by [17]

$$e^{-\frac{\pi}{2}(t\Delta f)^2} \tag{3.17}$$

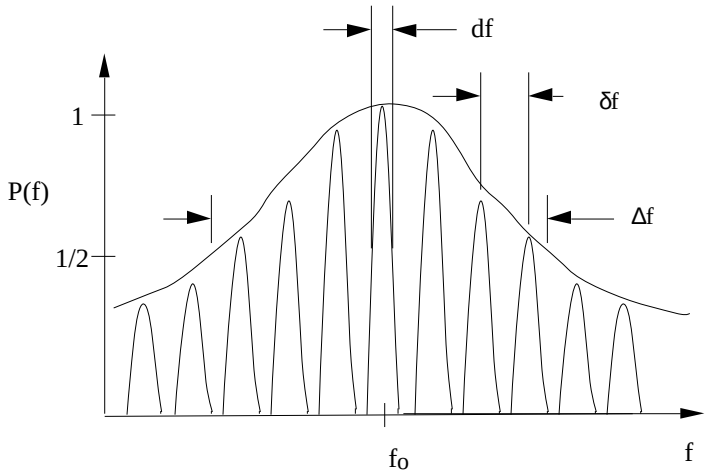

Figure 3.9 Typical spectrum of a multilongitudinal laser diode.

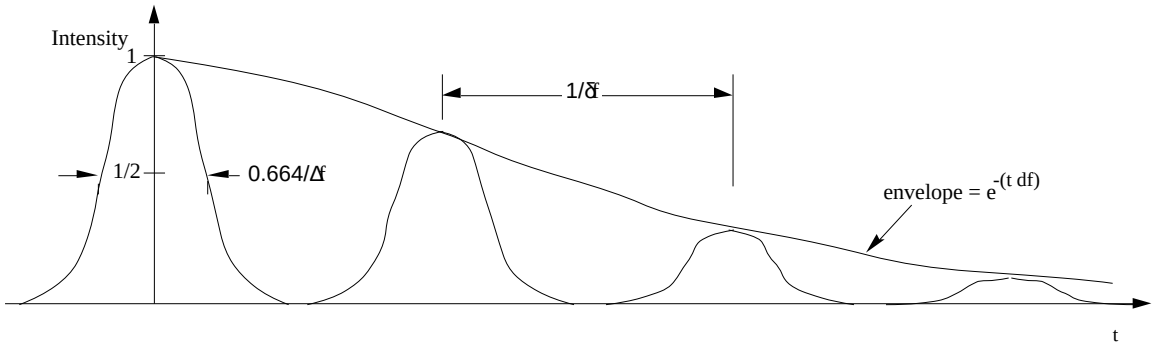

Figure 3.10. Envelope of fringe output with a multilongitudinal mode laser source.

With this in mind, the EFPI sensor must be designed so that the gap changes inside one of the interference zones, and preferably centered around the a peak to maximize the signal to noise ratio.

Chapter 4 - Experimental Results

In this chapter, we describe the experimental setup for the testing of the EFPI with a wavelength modulated source. Some of the limitations caused by the set-up are also discussed. Experiments are then performed to predict and verify the output interference zones of the multilongitudinal mode laser diode and the maximum modulation frequency of the laser diode. The performance of the EFPI with a wavelength modulated source is then analyzed and compared to other sensing schemes.

4.1 Experimental Setup

To test the operation of the EFPI with a wavelength modulated source, the following experiments were performed using the set-up described.

For all experiments, the ML7781A multilongitudinal mode laser diode was mounted to a temperature controlled heat sink (Figure 4.1). The thermoelectric controller maintained the temperature with 0.01° C. The source was driven with a low noise current driver that was modulated using a function generator. The current driver was used to set the DC bias point of the laser diode (I_{bias}), and the function generator voltage output was adjusted in amplitude and frequency for the various experiments (Figure 4.2). I_1 and I_2 establish the peak to peak current deviation, defining

$$I_{\text{mod}} = I_2 - I_1 . \tag{4.1}$$

The laser diode current was modulated at 0.1 mA/mV of input voltage to the current driver. The output was either a sawtooth modulation waveform or a triangular waveform.

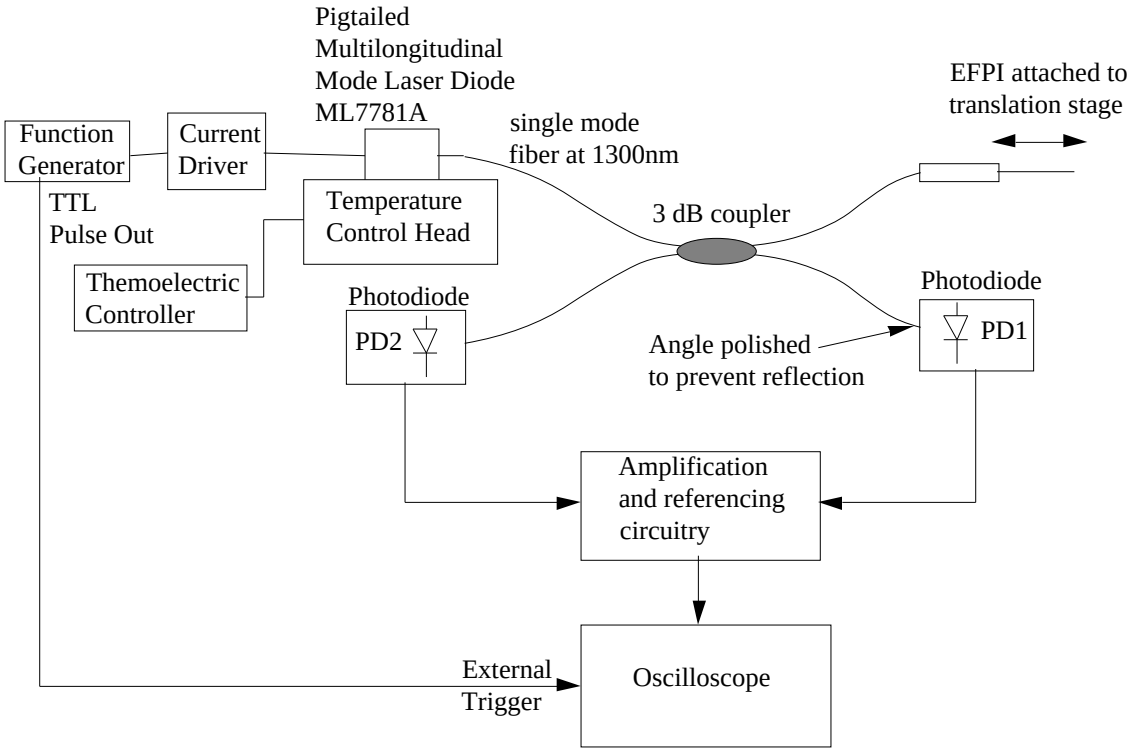

Figure 4.1 Overall experimental set-up for testing EFPI with a wavelength modulated source.

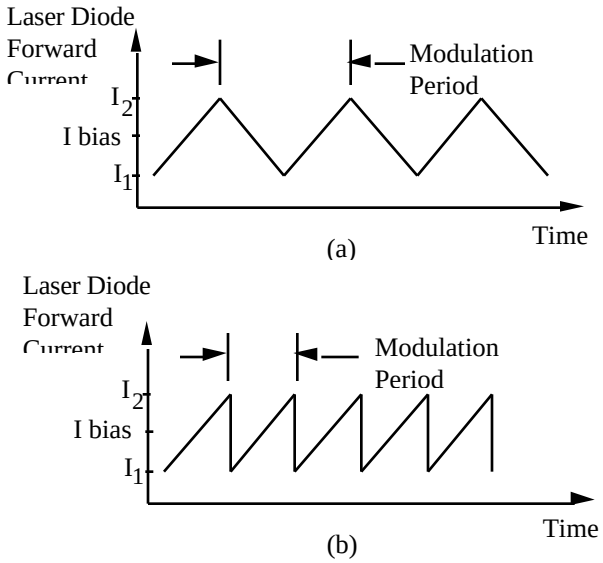

Figure 4.2. Current driver output modulation waveforms, (a) triangular modulation, and (b) sawtooth modulation.

When the forward current of a laser diode is modulated, the cavity gain also changes and results in an output intensity modulation in addition to the wavelength modulation. Figure 4.3 shows the output at PD2. A referencing circuit was employed to remove the unwanted intensity modulation and retrieve the fringe output in real time (Figure 4.4)[20]. By monitoring the intensity modulation with PD1, we can remove the intensity modulation by dividing the PD2 signal by the PD1 signal, also shown in Figure 4.3.

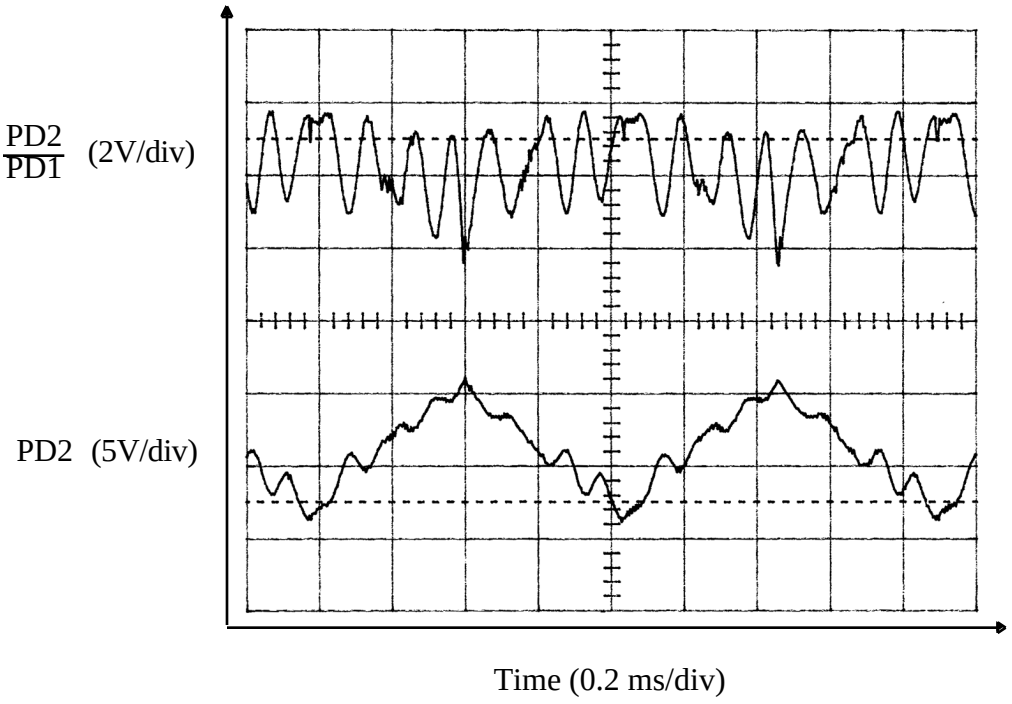

Figure 4.3. Output of PD2 and PD2/PD1

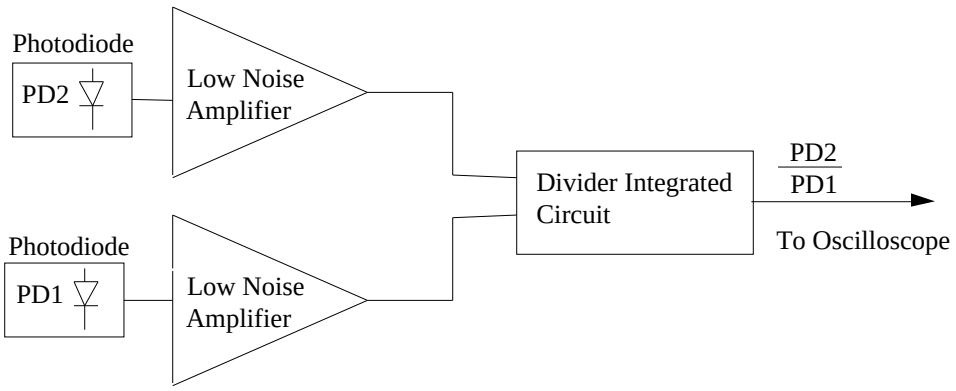

Figure 4.4. Amplification and referencing circuit

4.2 EFPI configurations

Three types of EFPI configurations were used in these experiments (Figure 4.5). The first configuration, described earlier as the extended-gap EFPI was compared to the traditional EFPI with a large gap and an extended-gap EFPI with a gold coating on the end of the reflector fiber. The gold coating provides a high reflectance end to increase the intensity of the sensing reflection.

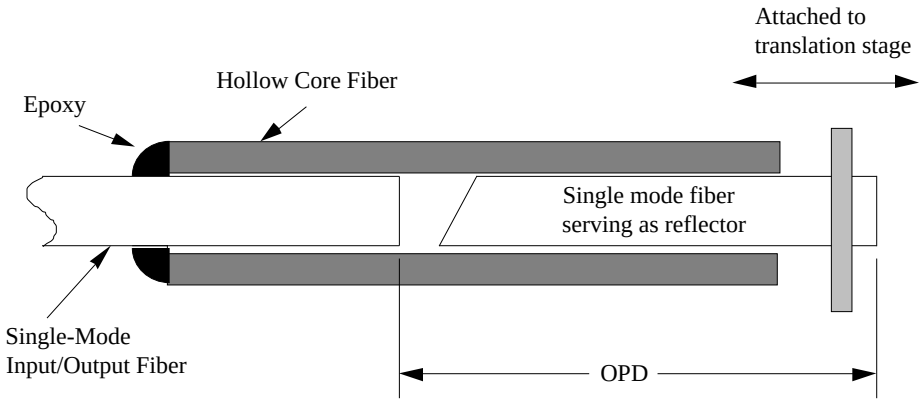

(a) Extended-gap EFPI

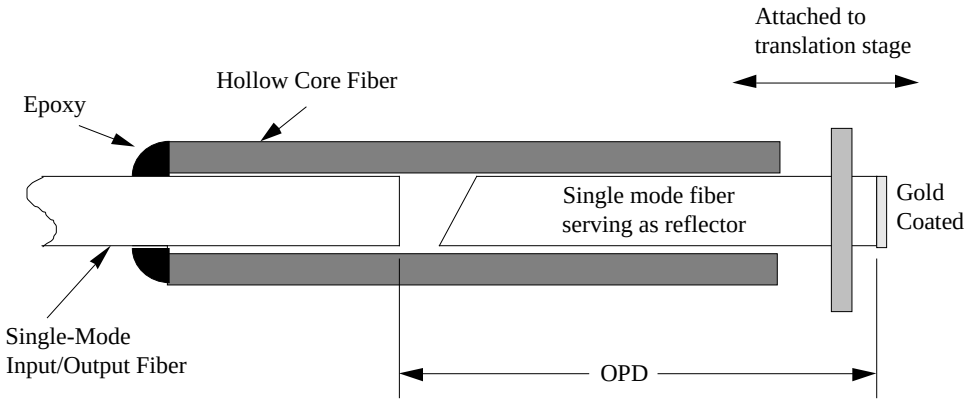

(b) Extended-gap EFPI with gold coated end

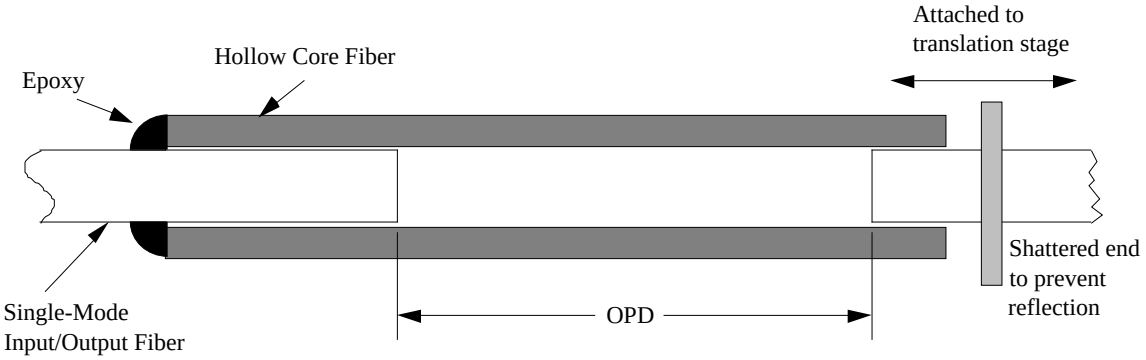

(c) Traditional EFPI with 90° fiber endface serving as reflector

Figure 4.5. Three EFPI configurations used in these experiments

4.3 Limitations of experimental setup

The testing of the EFPI with a wavelength modulated source was limited by the translation stages and the amplifying and referencing circuits. Two different translation stages were used. For large gap change measurements, a translation stage with 10 μm resolution was used, for small gap change measurements a translation stage with 0.5 μm resolution was used. The frequency response of the amplifying and referencing circuits was also limited. At frequencies approaching 100 kHz, the gain of the circuit began to fall off.

4.4 Interference zones in EFPI output

As described in Section 3.5, the parameters of the laser diode were determined by using an optical spectrum analyzer (OSA). The OSA converts the input source into intensity versus wavelength, and therefore all values were converted to frequency using Equation (3.1). The measured parameters for the ML7781A laser diode at I_{bias}=70 mA and no current modulation are

$$\begin{aligned} d\lambda &= 0.11nm & df &= 1.94\text{x}10^{10}\,Hz \\ \delta\lambda &= 0.75nm & \delta f &= 1.32\text{x}10^{11}\,Hz\ . \\ \Delta\lambda &= 5.0nm & \Delta f &= 8.82\text{x}10^{11}\,Hz \end{aligned} \qquad (5.1)$$

The output pattern consists of a series of equally spaced interference zones with FWHM of 0.664/Δf, spaced at 1/δf, and with an overall decreasing envelope according to the mode coherence time (1/df). If we convert the time values to distance by multiplying by the speed of light, the predicted output pattern will appear as shown in Figure 4.6.

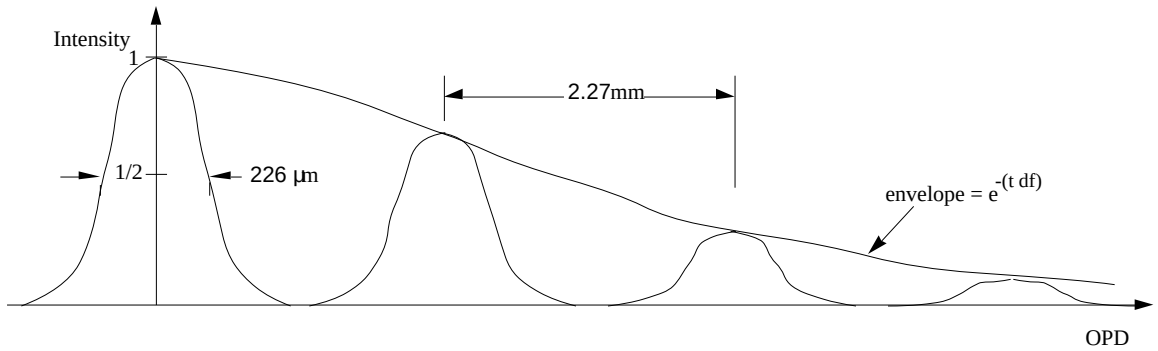

Figure 4.6. Predicted output of interference fringe zones using measured laser diode parameters

Although these calculations are useful for providing a general picture of the interference output pattern, they may not be accurate enough. The assumption of Gaussian and Lorenztian distribution of the modes does not hold and may cause large errors in the predicted output. From Figure 4. **7**, the output spectrum is not evenly distributed.

To more accurately predict the fringe output, the OSA was used to obtain a scan of the source spectral components from 1249 nm to 1359 nm, which consisted of 11 scans at the maximum resolution of 0.1 nm. The result was downloaded to a file of 6380 points of data that contained the intensities of light across the 110 nm bandwidth (Figure 4. **8**). To obtain the interference pattern, a program was written to perform the fast Fourier transform (FFT) of the spectrum data file. The result is an envelope of the interference pattern from 0 to 4.93 cm OPD with a resolution of 15.4 μm (Figure 4. **9**).

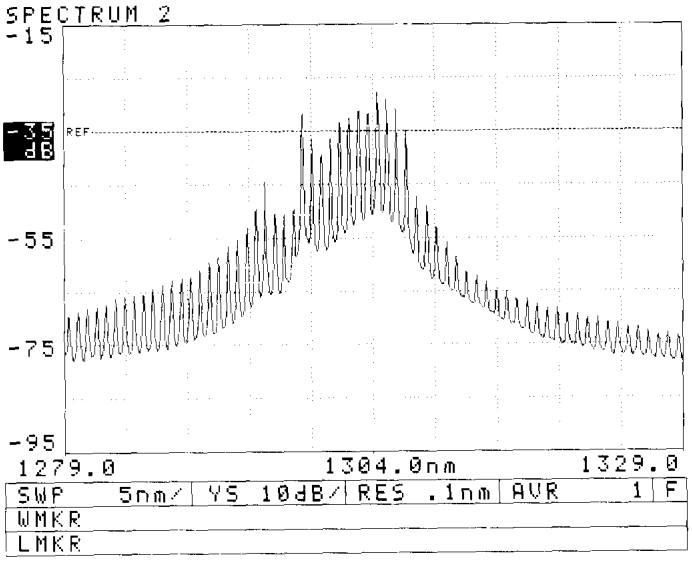

Figure 4. 7. Spectrum of ML7781A with I_{bias} = 70 mA.

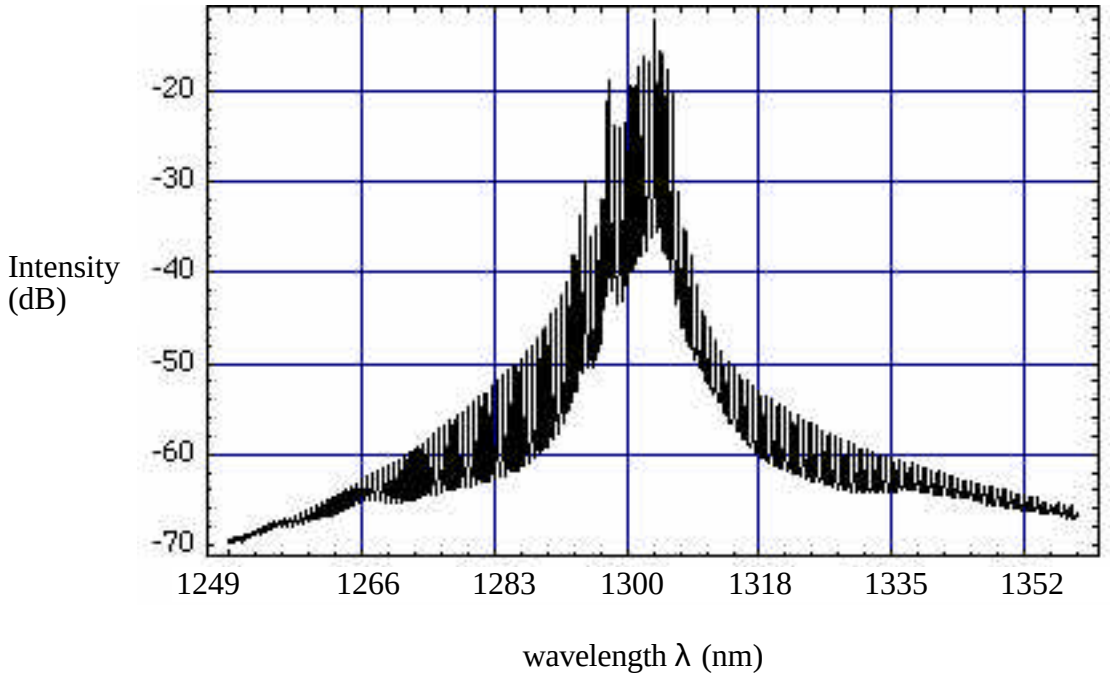

Figure 4. 8. Plot of 6380 data points used for performing FFT to determine interference zones.

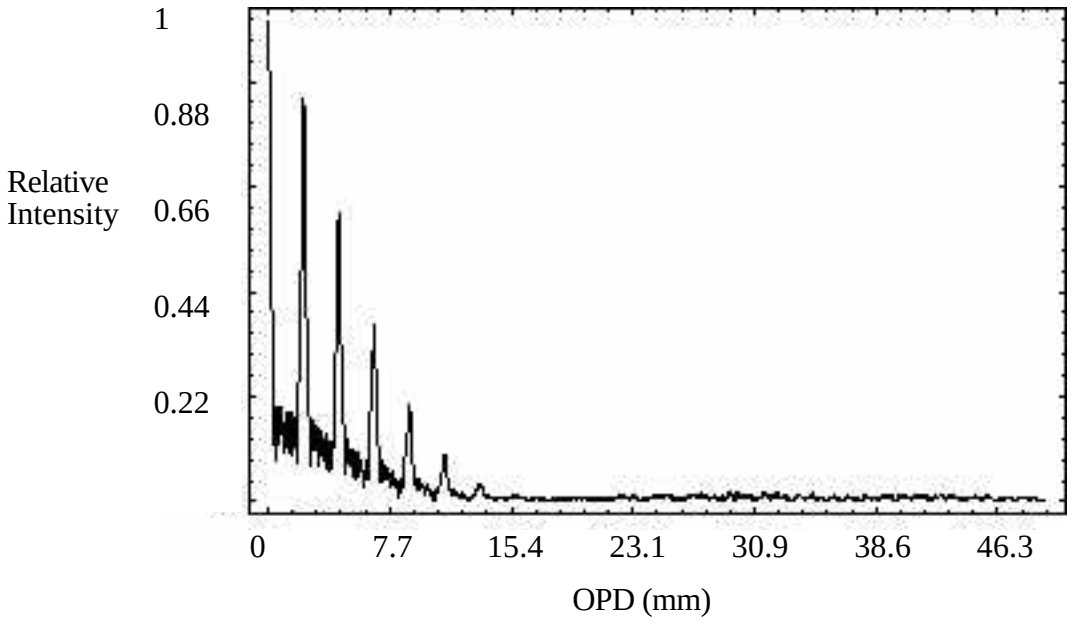

Figure 4. 9. Calculated interference zones for ML7781A at I_{bias} = 70 mA

Figure 4. **10** and Figure 4. **11** compare the calculated and measured interference zones. Figure 4. **11** was acquired using the setup shown in Figure 4.5 (c). The endface was manually scanned and the locations of the interference zone peaks noted. A close correlation between the calculated and measured location of the zones is achieved. Knowing the interference zones and their position allows the proper design of the EFPI to maximize the signal to noise ratio.

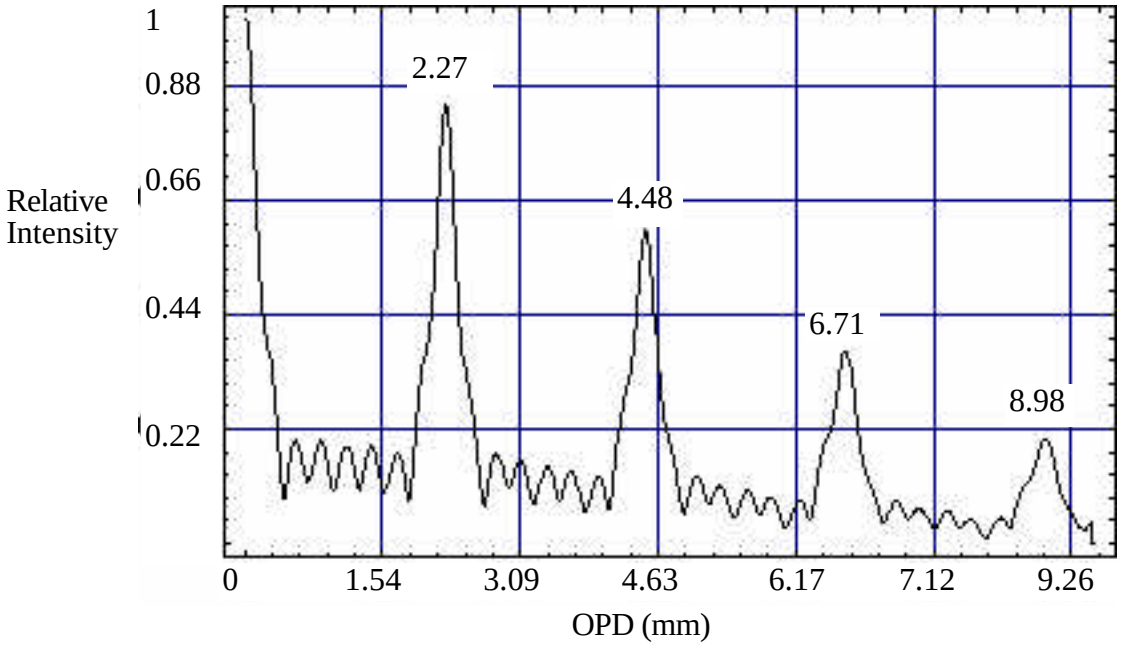

Figure 4. 10. Calculated interference zones for ML7781A from OPD of 0 to 9.5 mm at I_{bias} = 70 mA

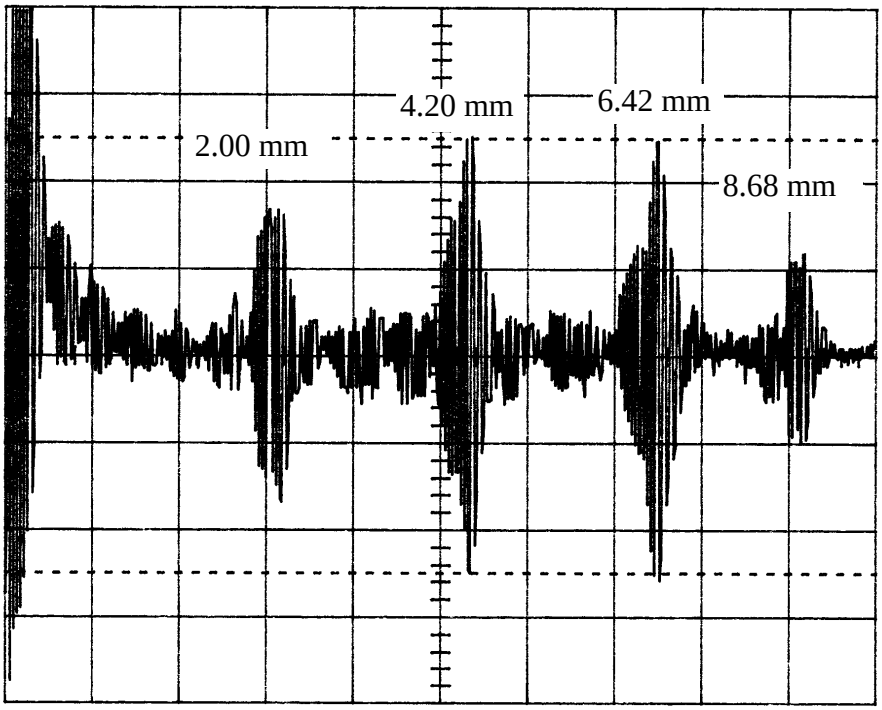

Figure 4. 11. Measured interference zones by manually scanning the OPD from 0 to 9.5 mm

4.5 Minimum gap and maximum frequency characteristics

Before testing the EFPI with a wavelength modulated source, the minimum usable gap and maximum current modulation had to be determined. Using a reflector fiber with a 10° polished endface and a shattered end, the fringe output was monitored while scanning the gap from 0 to 430 μm. At a gap length of 220 μm, the fringe output was negligible. This establishes the minimum usable gap distance to prevent interference with the reflections at the polished fiber endface.

To determine the maximum modulation frequency, the number of output fringes were monitored for a fixed peak to peak I_{mod} as the current modulation frequency f_{mod} was increased. As f_{mod} increases, the wavelength deviation caused by thermal effects begin to subside and the charge carrier induced refractive index change begins to dominate. As a result, the number of fringes for the same I_{mod} decreases. This effect is shown in Figure 4. **12**. A gold coated reflector fiber of 1.5cm length was used for this test and I_{mod} was 40 mA at an I_{bias} of 55 mA. As f_{mod} increases, the number of fringes decreases because the thermal effect is reduced. In addition, at frequencies above 10 kHz, the gain of the amplification and

dividing circuits decreases. As a result, the current system is limited to f_{mod} frequencies less than 10 kHz.

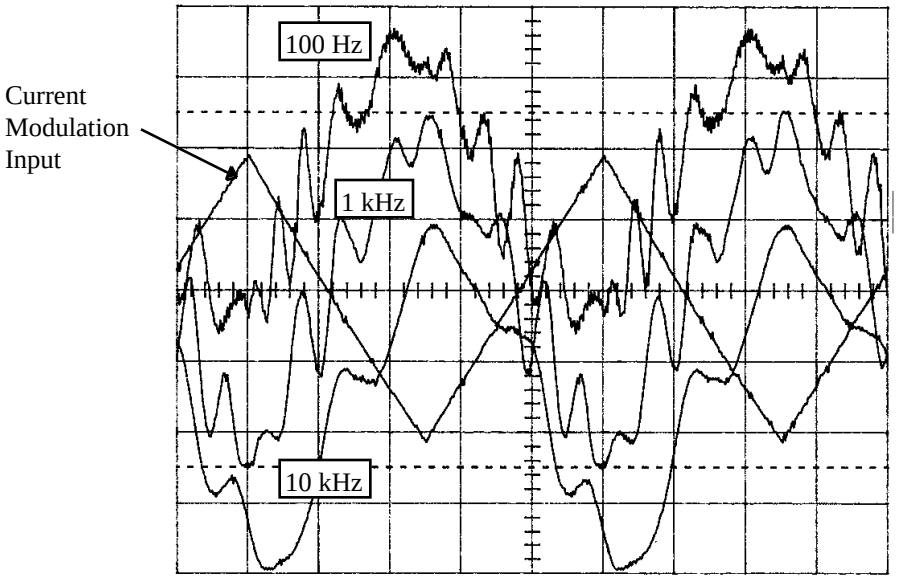

Figure 4. 12. Output at PD2 for three different f_{mod} frequencies: 100 Hz, 1 kHz, 10 kHz. I_{mod} is 40 mA. The middle graph is the triangular wave input to the current driver.

4.6 System Operational Characteristics

Using an extended gap EFPI geometry, the system was tested for a range of gap lengths. A 1.5 cm long gold coated reflector fiber was positioned at the beginning of an interference zone and the gap was slowly increased. The position of the peak of one fringe was monitored using the oscilloscope. This is illustrated in Figure 4. **13**. As the peak moved, every 2π phase change was recorded versus the change in the gap. The results for a small change in gap are shown in Figure 4. 14. The straight line is the theoretically predicted output from Equation (3.9).

Results for the same configuration taken over a larger change in gap are shown in Figure 4. **15** along with the theoretically predicted output.

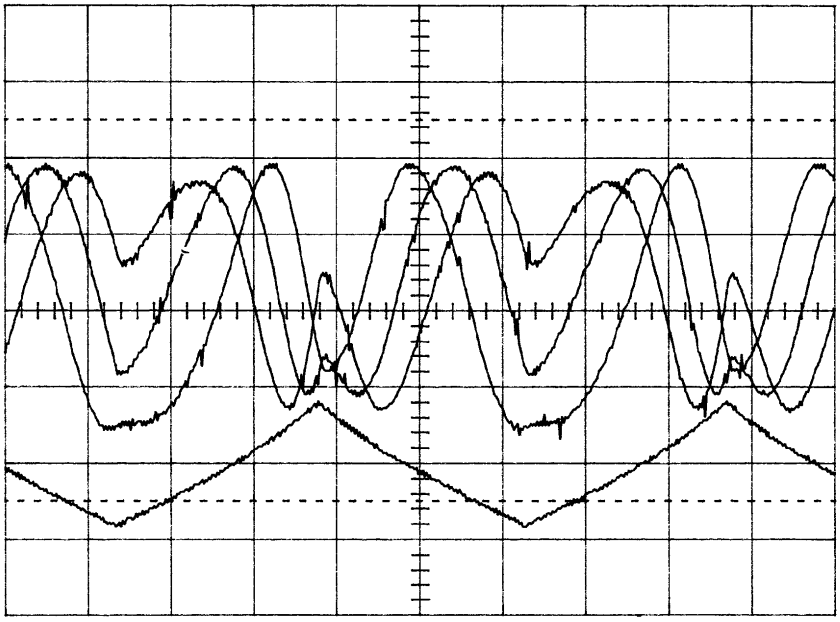

Figure 4. 13 Output showing the phase movement as the gap changes

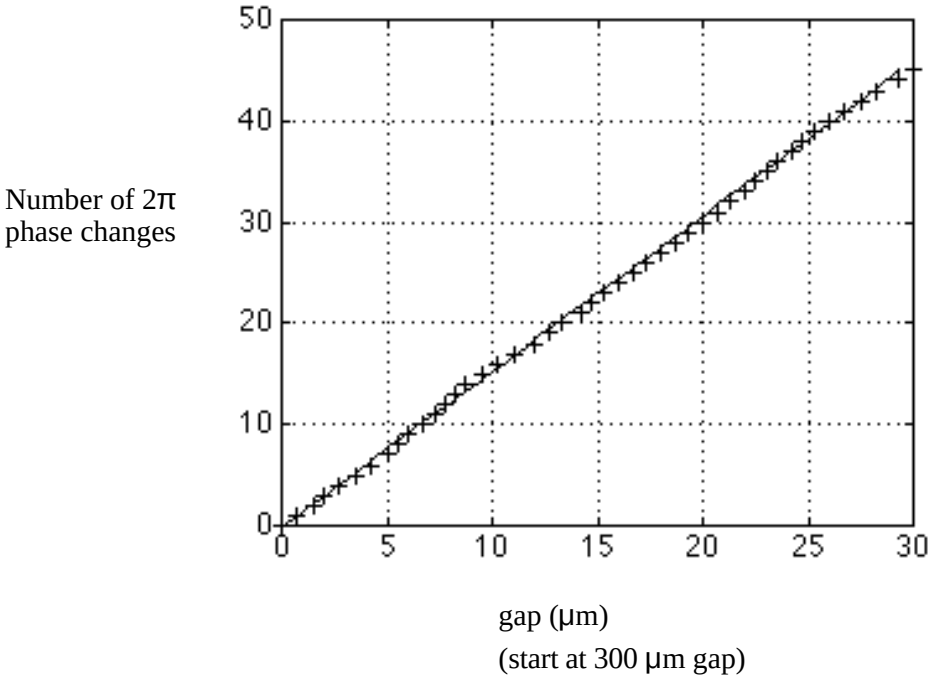

Figure 4. 14. Phase change vs. gap for extended-gap EFPI with wavelength modulated source.

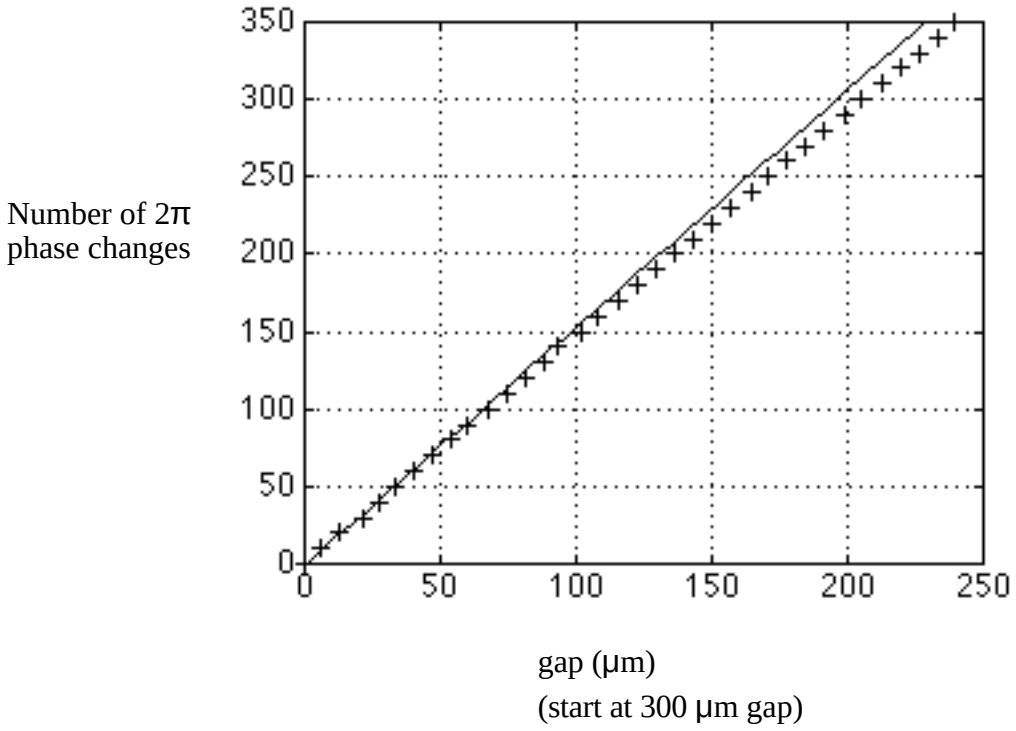

Figure 4. 15. Phase change vs. gap for extended-gap EFPI with wavelength modulated source.

4.7 Specifications and limitations of system

The results show a close correlation between the predicted and measured phase change. What is not clear from the data is the errors caused by phase drift. The signal contained a slow drift in phase of approximately ± π/4 radians. For a static measurements, this causes error and determines the minimum detectable change in gap.

The extended-gap EFPI employed as a strain sensor would have a gauge length of approximately 1.75 cm. Assuming a maximum strain before failure in the hollow core of 1.5%, this corresponds to a required dynamic range for the system of 263 μm. As shown in Figure 4. **15**, this range is achievable with this system. With a gap resolution of π/2 radians and 1.75 cm gauge length, the minimum detectable change in gap is 0.1625 μm and minimum detectable strain is 9.28 μstrain. This resolution would be significantly reduced in the presence of temperature fluctuations, and therefore a temperature compensation

scheme is required. An alternative is using the configuration shown in Figure 4.5 (c), which is much less susceptible to temperature fluctuations, but requires a larger gauge length. The disadvantage of this configuration is its sensitivity to reflector fiber endface lateral movement.

The present system's dynamic response is limited by the maximum capable f_{mod} of 10 kHz. Using the present set-up, the dynamic response could not be measured. As long as the phase movement is an order of magnitude less than f_{mod}, then the gap change should be measurable if a continuous real time phase tracking scheme were employed. Schemes to increase the wavelength deviation at higher f_{mod} could improve the dynamic response [14].

Chapter 5 - Conclusions and Future Work

5.1 Conclusions

A new type of signal demodulation system was developed for the EFPI. Using a wavelength modulated source and an extended-gap configuration, the following goals have been met:

1) Eliminated the need for complex fringe counting.
2) Reduced the effect of intensity modulations on the signal.
3) Moderate dynamic response.
4) Maintained a simple cost effective design.
5) Eliminated directional ambiguity.

Although these goals have been met, some system limitations will prevent it from becoming a practical design. The limitations are primarily reduced accuracy caused by temperature fluctuations and phase noise from the source. A temperature compensation scheme must be utilized in order to make this a viable signal demodulation scheme.

5.2 Future Work

To solve the problems discovered in this work, a different approach can be implemented using a broadband high-power source such as a super luminescent diode (SLD). The output of this device can be fed into a scanning bandpass filter (Figure 5.1). Given the FWHM of the SLD of 25 nm, the bandpass filter can scan a narrow portion of the broadband light at the input to the coupler. The combination of the two devices functions as a single mode device with a 25 nm scanning range.

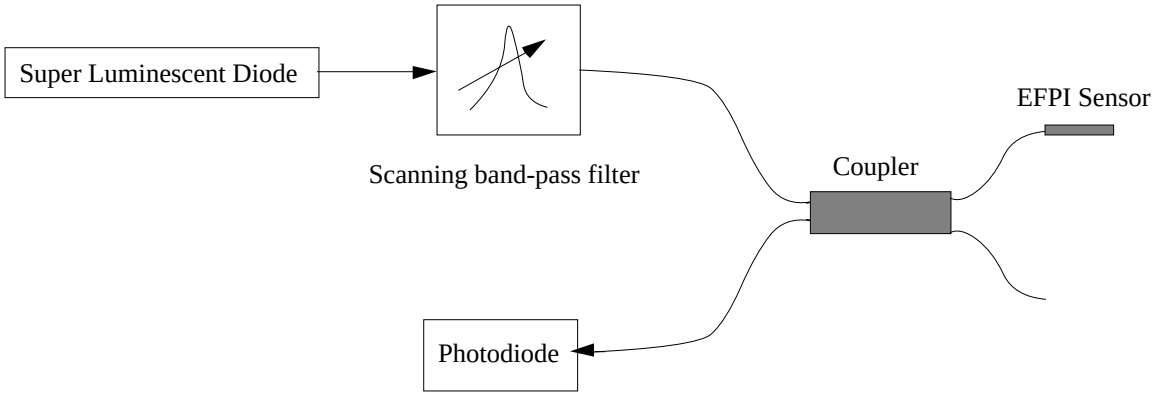

Figure 5.1. EFPI sensor system using broadband source and scanning bandpass filter

Using Equation (3.7), for one fringe period to appear at the output, the OPD required is 67.6 μm. Therefore, the gauge length has been reduced and an extended-gap configuration does not have to be implemented.

References

1. E. Udd, Fiber Optic Sensors: An Introduction for Engineers and Scientists, John Wiley and Sons, NY, 1991.

2. Scott Quist, Vincent Martinelli, and Ray Ikeda, "Fiber-Optic Gyroscopes in Automotive and Industrial Applications," *Sensors*, Vol. 13, No. 4, pp. 42-46, April 1996.

3. Peter L. Fuhr and Dryver R. Huston, "Fiber Optic Smart Civil Structures," *SPIE Proceedings*, Vol. 2574, pp. 6-11, May 1995.

4. Marten de Vries, "Optical fiber sensors for advanced civil structures," *Doctoral Dissertation*, Virginia Polytechnic Institute and State University, Blacksburg, VA, 1994.

5. J. Wilson and J. F. Hawkes, Optoelectronics, Prentice Hall, NY, 1989.

6. John W. Berthold III, "Historical Review of Microbend Fiber-Optic Sensors," *Journal of Lightwave Technology*, Vol. 13, pp. 1193-1199, July 1995.

7. S. Meller, M. J. de Vries, V. Arya, K. Murphy, R. O. Claus, "Optical Fiber Sensors for Vehicle Detection," *SPIE Proceedings*, Vol. 2592, pp. 39-45, October 1995.

8. J.L. Santos, A.P. Leite, and D.A. Jackson, "Optical fiber sensing with a low-finesse Fabry-Perot cavity," *Applied Optics*, Vol. 31, No. 34, pp.7361-7366, December 1992.

9. Kent A. Murphy, Michael F. Gunther, Ashish M. Vengsarkar, and Richard O. Claus, "Quadrature phase-shifted, extrinsic Fabry-Perot optical fiber sensors," *Optics Letters*, Vol.16, No. 4, pp.273-275, February 1991.

10. Kent Murphy, "Novel phase-modulated optical fiber sensors," *Doctoral Dissertation*, Virginia Polytechnic Institute and State University, Blacksburg, VA, 1992.

11. Vikram Bhatia, "Signal Processing Techniques for Optical Fiber Sensors Using White Light Interferometry," *Master's Thesis*, Virginia Polytechnic Institute and State University, Blacksburg, VA, 1993.

12. Asif Malik, "A Dual Wavelength Fiber Optic Strain Sensing System," *Master's Thesis*, Virginia Polytechnic Institute and State University, Blacksburg, VA, 1996.

13. John Dakin and Brian Culshaw, Optical Fiber Sensors: Principles and Components, Artech House, Boston, MA, 1988.

14. D.J. Anderson, J.D.C. Jones, P.G. Sinha, S.R. Kidd, and J.S. Barton, "Scheme for Extending the Bandwidth of Injection-current-induced Laser Diode Optical Frequency Modulation," *Journal of Modern Optics*, Vol. 38, No. 12, pp.2459-2465, 1991.

15. George Economou, R.C. Youngquist, and D.E.N. Davies, "Limitations and Noise in Interferometric Systems Using Frequency Ramped Single-Mode Diode Lasers," *Journal of Lightwave Technology*, Vol. LT-4, No.11, November 1986.

16. Koichi Iiyama, Lu-Tang Wang, and Ken-ichi Hayashi, "Linearizing Optical Frequency-Sweep of a Laser Diode for FMCW Reflectometry," *Journal of Lightwave Technology*, Vol. 14, No. 2, February 1996.

17. K. Oka, M. Tsukada, and Y. Ohtsuka, "Real-time phase deomdulator for optical heterodyne detection processes," *Journal of Physics E: Measuremnt Science Technology*, Vol. 2, pp. 106-110, 1991.

18. W.C. Young, V. Shah, L. Curtis, "Loss and Reflectance of Standard Cylindrical-Ferrule Single-Mode Connectors Modified by Polishing a 10° Oblique Endface Angle," *IEEE Photonics Technology Letters*, Vol. 1, No. 12, pp.461-463, December 1989.

17. Awad Samir Gerges, T.P. Newson, and D.A. Jackson, "Coherence tuned fiber optic sensing system, with self-initialization, based on a multimode laser diode," *Applied Optics*, Vol. 29, No. 30, pp.4473-4480, October 1990.

18. K.D. Moller, Optics, University Science Books, Mill Valley, CA, 1988.

19. Jean-Pierre Goedgebuer, Henri Porte, and Andre Hamel, "Electrooptic modulation of multilongitudinal mode laser diodes: demonstration at 850 nm with simultaneous data transmission by coherence multiplexing," *IEEE Journal of Quantum Electronics*, Vol. QE-23, No. 7, pp. 1135-1144, July 1987.

20. G. Beheim and K. Fritsch, "Remote Displacement Measurements using a Laser Diode," *Electronics Letters*, Vol. 21, No. 3, pp. 93-94, January 1985.

21. Hisao Kikuta, Koichi Iwata, Ryo Nagata, "Distance measurement by the wavelength shift of laser diode light," *Applied Optics*, Vol. 25, No. 17, pp.2976-2980, September 1986.

22. Pie-Yau Chien, Yau-Sheng Chang, and Ming-Wen Chang, "Distance and velocity detection interferometer by using a frequency triangular-modulated laser diode," *Applied Optics*, Vol. 34, No. 16, pp.2853-2855, June 1995.

23. Zhao Yang and Li Da-Cheng, "Signal processing of fiber displacement sensor with linear frequency modulation laser diode," *SPIE Proceedings*, Vol. 2101, pp. 1208-1212, 1993.

24. Vivek Arya, Marten J. de Vries, Madhu Athreya, Anbo Wang, Richard O. Claus, "Analysis of the effect of imperfect fiber endfaces on the performance of extrinsic Fabry-Perot interferometric optical fiber sensors," *Optical Engineering*, Vol. 35, No. 8, pp. 2262-2265, August 1996.

Vita

Scott Meller was born in St. Charles, Missouri on February 23, 1967. He graduated with a Bachelor of Science degree in Electrical Engineering from Clemson University in 1989. He then worked at Naval Undersea Warfare Center Detachment Norfolk in the surface ship torpedo defense program. In 1995, he joined Fiber and Electro-Optics Research Center at Virginia Tech as a Graduate Research Assistant. He earned his Master of Science degree in Electrical Engineering from Virginia Tech in December 1996. Scott Meller is currently a employed at F&S Inc. as a Research Scientist in Blacksburg, VA.